Phys. Lett. B 866 (2025) 139526

Contents lists available at ScienceDirect

Physics Letters B

journal homepage: www.elsevier.com/locate/physletb

Letter

Measurement of the Drell–Yan forward-backward asymmetry and of the effective leptonic weak mixing angle in proton-proton collisions at $\sqrt{s} = 13$ TeV

The CMS Collaboration *

CERN, Geneva, Switzerland

ARTICLE INFO

Editor: M. Doser

Keywords:
CMS
Electroweak
Mixing angle
Drell-Yan

ABSTRACT

The forward-backward asymmetry in Drell–Yan production and the effective leptonic electroweak mixing angle are measured in proton-proton collisions at $\sqrt{s} = 13$ TeV, collected by the CMS experiment and corresponding to an integrated luminosity of 138 fb^{-1}. The measurement uses both dimuon and dielectron events, and is performed as a function of the dilepton mass and rapidity. The unfolded angular coefficient A_4 is also extracted, as a function of the dilepton mass and rapidity. Using the CT18Z set of parton distribution functions, we obtain $\sin^2\theta^{\ell}_{\text{eff}} = 0.23152 \pm 0.00031$, where the uncertainty includes the experimental and theoretical contributions. The measured value agrees with the standard model fit result to global experimental data. This is the most precise $\sin^2\theta^{\ell}_{\text{eff}}$ measurement at a hadron collider, with a precision comparable to the results obtained at LEP and SLD.

1. Introduction

The electroweak (EW) mixing angle, relating the masses of the W and Z bosons (m_{W} and m_{Z}), $\sin^2\theta_{\text{W}} = 1 - m^2_{\text{W}}/m^2_{\text{Z}}$, is a key parameter in the standard model (SM) of particle physics. It defines the ratio between the vector and axial-vector couplings of the Z boson with fermions, $v_{\text{f}}/a_{\text{f}} = 1 - 4|Q_{\text{f}}|\sin^2\theta_{\text{W}}$, where Q_{f} is the electric charge of the fermion f. Although EW radiative corrections change this tree-level picture, the same relation can be kept for all orders by introducing an effective mixing angle that depends on the fermion flavor. Both m_{W} and the effective leptonic mixing angle ($\sin^2\theta^{\ell}_{\text{eff}}$) can be precisely obtained in the SM, using LEP and SLD measurements at the Z resonance [1], the muon lifetime, and the masses of the top quark and of the Higgs boson. The current predictions, from a global EW fit [2], are $m_{\text{W}} = 80\,360 \pm 6$ MeV and $\sin^2\theta^{\ell}_{\text{eff}} = 0.23155 \pm 0.00004$. Measurements of m_{W} and $\sin^2\theta^{\ell}_{\text{eff}}$ provide an important test of the SM since deviations from the predictions could be evidence of beyond-the-SM physics. Currently, the most precise $\sin^2\theta^{\ell}_{\text{eff}}$ values are 0.23221 ± 0.00029, from b quark forward-backward asymmetry ($A^{0,\text{b}}_{\text{FB}}$) results at the CERN LEP experiments, and 0.23098 ± 0.00026, from left-right asymmetry (A^{0}_{LR}) data at the SLD experiment at SLAC [1]. These two values differ by 3.2 standard deviations. This Letter presents a $\sin^2\theta^{\ell}_{\text{eff}}$ measurement with a precision that exceeds that of all previous hadron collider measurements [3–14] and is comparable to that of the LEP and SLD results [1].

In proton-proton (pp) collisions at the CERN LHC, Drell–Yan (DY) production is driven by the vector and axial-vector couplings of the Z boson to fermions. We measure $\sin^2\theta^{\ell}_{\text{eff}}$ using $\text{pp} \to Z/\gamma + X \to \ell^+\ell^- + X$ events, where the $\ell^+\ell^-$ dilepton invariant mass is near the Z boson mass and ℓ is either a muon or an electron. To reduce theoretical and experimental uncertainties, we use leptonic angular distributions in the Collins–Soper (CS) frame [15]. The angle of the negatively charged lepton relative to the incoming quark direction, θ_{CS}, is computed as

$$\cos\theta_{\text{CS}} = \frac{2\left(Q_1^+ Q_2^- - Q_1^- Q_2^+\right)}{\sqrt{m^2(m^2 + p_{\text{T}}^2)}} \frac{y}{|y|},$$

where m, p_{T}, and y are the mass, transverse momentum, and rapidity of the dilepton, respectively, and $Q_i^{\pm} = (E_i \pm P_{z,i})/\sqrt{2}$, with E and P_z being the energy and longitudinal momentum of the leptons, with $i = 1$ for ℓ^- and 2 for ℓ^+. In this equation, y is used as a proxy for the valence quark direction. Before final-state radiation (FSR), the DY differential cross section for the polar (θ) and azimuthal (ϕ) decay angles can be described [16] as

$$\frac{16\pi}{3\sigma}\frac{\text{d}\sigma}{\text{d}\cos\theta\,\text{d}\phi} = 1 + \cos^2\theta + \sum_{i=0}^{7} A_i f_i(\theta,\phi),$$

* *E-mail address:* cms-publication-committee-chair@cern.ch.

https://doi.org/10.1016/j.physletb.2025.139526
Received 14 August 2024; Received in revised form 14 April 2025; Accepted 29 April 2025
Available online 7 May 2025
0370-2693/© 2025 CERN for the benefit of the CMS Collaboration. Published by Elsevier B.V. Funded by SCOAP³. This is an open access article under the CC BY license (http://creativecommons.org/licenses/by/4.0/).

where σ is the unpolarized cross section and $f_0 = 0.5(1 - 3\cos^2\theta)$, $f_1 = \sin 2\theta \cos\phi$, $f_2 = 0.5\sin^2\theta\cos 2\phi$, $f_3 = \sin\theta\cos\phi$, $f_4 = \cos\theta$, $f_5 = \sin^2\theta\sin 2\phi$, $f_6 = \sin 2\theta \sin\phi$, and $f_7 = \sin\theta\sin\phi$. The angular coefficients A_i are functions of the mass (M), transverse momentum (P_T), and rapidity (Y) of the pre-FSR dilepton. Except for the forward-backward asymmetry coefficient, A_4, all the angular coefficients are small. Integrating the cross section over ϕ, the dependence on $\cos\theta$ is fully described by the A_0 and A_4 coefficients. In this analysis, we also integrate over P_T.

The $\sin^2\theta^{\ell}_{\text{eff}}$ analysis of $\sqrt{s} = 8$ TeV CMS data [14] used the directly measured forward-backward angular-weighted asymmetry, A^{w}_{FB}, approximately equal to $A_{FB} = (\sigma_F - \sigma_B)/(\sigma_F + \sigma_B)$ in full phase space, where σ_F and σ_B are the $\cos\theta_{CS} > 0$ and $\cos\theta_{CS} < 0$ integrated cross sections, respectively. In full phase-space and before FSR, $A_{FB} = (3/8)\,A_4$. This angular-weighted asymmetry method [17], with weights that are functions of the rapidity and $\cos\theta_{CS}$ of the dilepton, uses reconstructed variables and benefits from the cancelation of systematic uncertainties in the detection acceptance and efficiencies, which are approximately identical for positive and negative $\cos\theta_{CS}$. In this Letter, we report a $\sin^2\theta^{\ell}_{\text{eff}}$ measurement with reduced uncertainties, obtained by applying this method to the larger $\sqrt{s} = 13$ TeV CMS data sample. We also report $\sin^2\theta^{\ell}_{\text{eff}}$ results obtained by fitting the unfolded angular coefficient A_4 as a function of the rapidity and mass of the pre-FSR dilepton. This second method, while more complex, provides a measurement with smaller theory and parton distribution function (PDF) uncertainties, which can be used in reinterpretations of the results (e.g., with improved PDFs) and in combinations with other measurements.

2. The CMS detector and data samples

The CMS apparatus [18,19] is a multipurpose and nearly hermetic detector, designed to trigger on [20,21] and identify electrons, muons, photons, and (charged and neutral) hadrons [22–24]. A global event description algorithm [25] aims to reconstruct all individual particles in an event, combining information provided by the all-silicon inner tracker and by the crystal electromagnetic (ECAL) and brass-scintillator hadron (HCAL) calorimeters, operating inside a 3.8 T superconducting solenoid, with data from the gas-ionization muon detectors embedded in the flux-return yoke outside the solenoid.

The ECAL and HCAL calorimeters provide the pseudorapidity coverage of $|\eta| < 3.0$, which is extended up to $|\eta| = 5$ by forward calorimeters that use quartz fibers as active material [26]; electromagnetic and hadronic showers can be distinguished by comparing the signals of long fibers that extend over the full depth of the detector with those of short fibers that start 22 cm into the detector. The reconstructed particles are used to build τ leptons, jets, and missing transverse momentum [27–29].

The measurement reported in this Letter is based on samples of pp collisions at $\sqrt{s} = 13$ TeV, collected by the CMS experiment in 2016–2018. The 2016 data sample is split in two, referred to as 2016a and 2016b, because of a change made to improve the hit efficiency of the silicon tracker at high instantaneous luminosities [30]. The integrated luminosities of the 2016a, 2016b, 2017, and 2018 data samples are 19.5, 16.8, 41.5, and 59.8 fb^{-1}, respectively, with 1.2–2.5% individual uncertainties [31–33].

The events are selected by dilepton and single-lepton triggers. Both triggers include a lepton isolation requirement. The dimuon trigger requires one muon with $p_T > 17$ GeV and another with $p_T > 8$ GeV, whereas the corresponding thresholds for the dielectron trigger are 23 and 12 GeV. The single-muon and single-electron triggers impose minimum p_T thresholds of 24 and 27 GeV (28 GeV in 2018), respectively. During part of the data-taking periods, these single-lepton triggers were prescaled, with the unprescaled triggers having higher p_T thresholds. The muons are reconstructed within the $|\eta| < 2.4$ range.

Three electron categories are considered, depending on the detectors involved in their reconstruction: central electrons (e), in the $|\eta|$ range covered by the silicon tracker; forward ECAL electrons (g), within $2.5 < |\eta| < 2.87$; and forward HCAL electrons (h) in the 3.14–4.36 $|\eta|$ range. We consider four dilepton categories: μμ, ee, eg, and eh. The central-central μμ and ee channels use both single-lepton and dilepton triggers, whereas the eg and eh central-forward channels only use single-electron triggers. In events with two or more central leptons satisfying the selection criteria, the central-central dileptons are composed of the two highest p_T leptons ("leading" and "trailing"). The two leptons are required to satisfy the kinematic requirements listed in Table 1, have opposite charges, and satisfy trigger-matching criteria: either they are both matched with dilepton trigger objects or one of them (with $p_T > 25$ GeV for muons and 30 GeV for electrons) is matched with a single-lepton trigger object. For the eh events, the central electron is required to be in the endcap ($|\eta| > 1.57$) to reduce background contamination.

Table 1
The lepton η and p_T acceptance windows applied in the four measurement channels. The 1.44–1.57 $|\eta|$ range, between the barrel and endcap ECAL, is excluded for central electrons.

	$\lvert\eta\rvert$		$p_{T,\text{min}}^{\text{leading}}$	$p_{T,\text{min}}^{\text{trailing}}$
μμ	0.00–2.40		20 GeV	10 GeV
ee	0.00–2.50		25 GeV	15 GeV
	$\lvert\eta_e\rvert$	$\lvert\eta_{g,h}\rvert$	$p_{T,\text{min}}^{e}$	$p_{T,\text{min}}^{g,h}$
eg	0.00–2.50	2.50–2.87	30 GeV	20 GeV
eh	1.57–2.50	3.14–4.36	30 GeV	20 GeV

The reconstructed muons are required to pass the "standard medium-identification" and "loose tracker isolation" criteria, with an efficiency of about 95% [23,34]. The central electron candidates must satisfy the cut-based "medium-identification criteria", including an isolation requirement, with an efficiency of about 80% [22]. In the eg and eh event classes, the central electron must also satisfy the "selective charge identification" criterion, which has about 95% efficiency and requires that three different charge determination methods give the same result (in ee events, this is not required, and each electron charge is determined by a "majority" rule [22]).

The g and h electrons are reconstructed and selected using independent procedures, to optimize their individual signal-selection efficiencies. Dedicated multivariate identification criteria, based on the shower shape and isolation variables, were developed for the g electrons. The cut-based working point with a signal selection efficiency of about 80% was derived using TMVA [35]. The h electrons are reconstructed from the constituents of jets built with the anti-k_T algorithm [36], using a cone radius of 0.4. Several reconstruction and identification algorithms were developed to optimally reconstruct the energy and direction of the prompt h electrons, and to distinguish them from the quark and gluon jets. In particular, we use multivariate classification and regression models implemented in TensorFlow [37], reaching better resolutions than with simpler methods. The input variables include, in addition to some pileup-sensitive variables, all the individual long and short fiber readout channels of each η-ϕ cell in a jet. Therefore, they contain isolation and shower shape (both transverse and longitudinal) information. The working point corresponds to an electron selection efficiency of about 70%. In the eg and eh classes, the two electrons must be in the same pseudorapidity hemisphere; the charge of the forward electron cannot be measured and is assumed to be the opposite of the charge of the central electron.

After applying the selection criteria described above, we retain about 111 million μμ, 59 million ee, 5.0 million eg, and 3.3 million eh events, including small background contaminations, as discussed in Section 5. The number of ee event is smaller than that of μμ given the lower electron selection efficiencies and higher electron p_T cuts, driven by the online trigger thresholds.

Fig. 1 shows how the dilepton mass resolution, at the Z mass, varies with absolute rapidity, for the four dilepton categories.

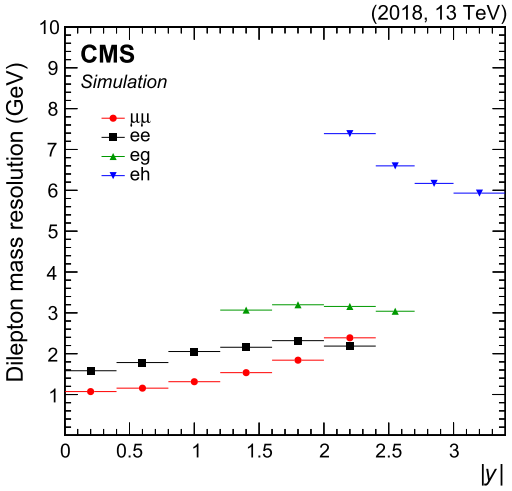

Fig. 1. Dilepton mass resolution, at the Z mass, as a function of the dilepton absolute rapidity, for the μμ, ee, eg, and eh channels.

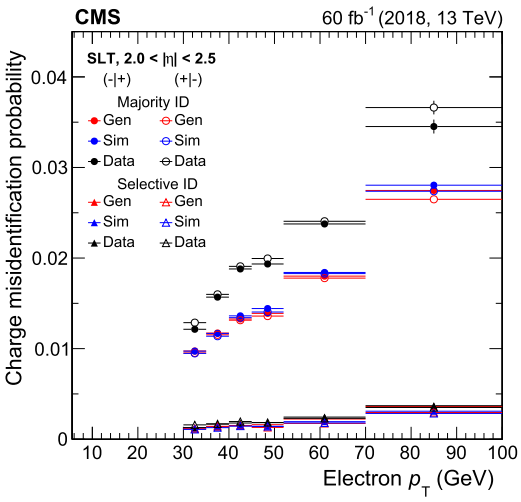

Fig. 2. Misidentification rates in the 2018 samples, for electrons in the $2.0 < |\eta| < 2.5$ bin that pass the single-lepton trigger (SLT): (1) majority (circles) and selective (triangles) charge identification; (2) misidentification of electrons as positrons (+|−) (open markers) or positrons as electrons (−|+) (solid markers); (3) true (red), simulation (blue), and data (black). The true charge misidentification rate is evaluated by counting electrons with wrong reconstructed charge using generation-level information; the simulated misidentification rate is evaluated with the method used in data.

3. Simulation and corrections

The signal and background processes are modeled using Monte Carlo (MC) simulation. The $Z/\gamma \to \ell\ell$ signal ($\ell = e, \mu$) and background ($\ell = \tau$) events are generated with the POWHEG 2.0 event generator [38,39], with a multi-scale improved next-to-next-to-leading order (MiNNLO$_{PS}$) accuracy in quantum chromodynamics (QCD) [40,41], matched with PYTHIA 8.2 [42] for the parton shower and hadronization steps, as well as for initial-state radiation. Photon FSR is simulated with the PHOTOS 2 package [43,44]. The signal events are generated with the next-to-next-to-leading order (NNLO) NNPDF3.1 PDF set [45]. Alternative event weights for variations of renormalization and factorization scales, PDF sets [46–48], and their uncertainties are also considered [49]. Additional small corrections to MiNNLO$_{PS}$ are described below.

Top quark pairs, s-channel single top events, and W+jets events are generated with the event generator MADGRAPH5_aMC@NLO 2.6.5 [50], at next-to-leading order (NLO) accuracy in QCD. The t-channel single top and tW events are generated with POWHEG, at NLO in QCD. The diboson event categories ZZ, WZ, WW, and $\gamma\gamma \to \ell\ell$ events are generated with PYTHIA 8 at leading order (LO). In all these cases, PYTHIA 8 is used to model the parton shower and hadronization steps, as well as initial and final state radiation. As discussed in Section 4, some of the backgrounds are evaluated using data driven methods and do not require MC samples.

The detector response is emulated with GEANT4 [51]. All the simulated final-state particles are reconstructed with the same algorithms as used for the measured data and the dilepton event candidates are selected with the criteria described in the previous section. Additional pp interactions in the same and nearby bunch crossings, "pileup", are included in the simulated samples, with weights based on the measured instantaneous luminosity and total inelastic cross section [52]. Various other corrections are applied to the simulated events. The signal $Z/\gamma \to \ell\ell$ events are generated at LO EW accuracy, with $\sin^2\theta^{\ell}_{\text{eff}}$, m_Z, and the Fermi constant G_μ as input parameters, and are corrected to account for NLO virtual weak corrections, including certain universal higher-order (HO) contributions, using POWHEG-Z_ew [53–55]. A large event sample is generated at NLO in QCD and LO in EW with the same EW input scheme as MiNNLO$_{PS}$ and including weights for the NLO+HO EW corrections. The dilepton $|y|$-m-p_T triple-differential cross sections and angular coefficients, calculated at LO and NLO+HO EW, are used to correct the corresponding MiNNLO$_{PS}$ predictions.

During the 2016 and 2017 data-taking periods, a gradual shift in the timing of the inputs of the ECAL L1 trigger in the $|\eta| > 2.0$ region caused a trigger inefficiency, denoted as "prefiring" [20,34]. The trigger missed between 10% and 20% of the events containing an electron (of $p_T \gtrsim 50$ GeV) or a jet (of $p_T \gtrsim 100$ GeV) in the $2.5 < |\eta| < 3.0$ range, the exact loss depending on the p_T and η of the trigger object. Correction factors were computed from data and applied to the acceptance evaluated by simulation.

The lepton selection efficiencies, in the measured and simulated events, are evaluated with the tag-and-probe method using $Z/\gamma \to \ell\ell$ events [56], separately for the reconstruction, identification, and trigger selection steps. In the case of the trigger, they are also evaluated separately for the prescaled and unprescaled single-lepton triggers, and for the two dilepton trigger legs. The event selection efficiency is computed from these individual components in p_T and η bins, accounting for the correlations between the single-lepton and dilepton trigger selection efficiencies, and also including a pileup-dependent factor for the prescaled single-lepton triggers. The ratio between the selection efficiencies in the measured and simulated samples is then applied as a weight to the simulated events.

The small electron charge misidentification rates for the "selective" and "majority" charge-identifications [22] are evaluated as a function of the electron p_T and $|\eta|$, with a maximum-likelihood fit, in the measured and simulated samples, using same-sign and opposite-sign dielectrons (at the Z peak). The electrons used for this purpose are also categorized depending on whether they pass the single-lepton trigger selection. Fig. 2 shows the misidentification rates for several configurations, using the 2018 samples for illustration. The misidentification rates in simulation ("Sim") agree well with the values obtained by counting the electrons with misidentified charge according to the generator information ("Gen"). As expected, the selective charge identification option leads to smaller misidentification probabilities than the majority option. The probabilities of misidentifying electrons as positrons and vice-versa are equal within uncertainties, for all data-taking periods. The charge misidentification rates in data and simulation are used to correct the simulation. The full correction, which is used as a conservative estimate of its uncertainty, has a negligible impact on this measurement. For dimuons, the charge misidentification is negligible [34].

We also correct the residual mismodeling of the dilepton p_T distributions with weights derived iteratively and applied to the pre-FSR simulated dilepton p_T, in bins of rapidity. The uncertainty associated with this correction is small and the full correction is assigned as a systematic uncertainty.

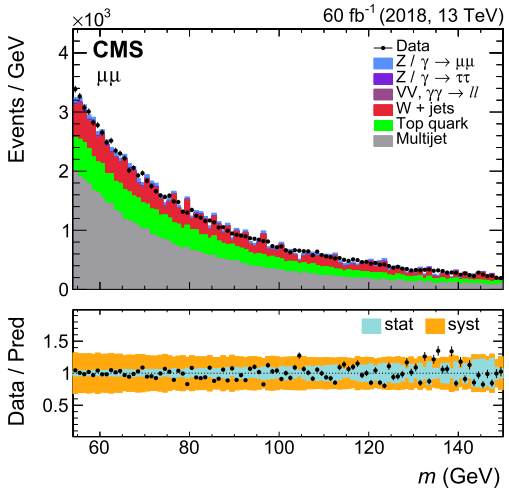

Fig. 3. Same-sign dimuon mass distribution for the 2018 sample. The EW and top quark backgrounds are normalized to the integrated luminosity using NNLO cross sections. The multijet background is evaluated by applying weights to the corresponding multijet-enriched samples. The error bars in the lower panel include statistical and background systematic uncertainties (described in Section 5).

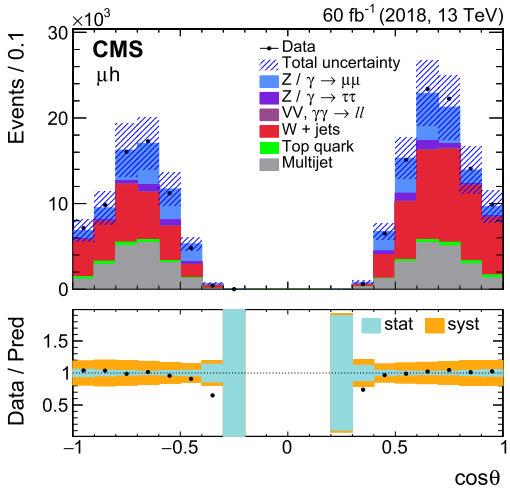

Fig. 4. Lepton $\cos\theta_{CS}$ distribution in μh events in 2018. The multijet and W+jets backgrounds are scaled to the data as described in the text. The error bars include statistical and background systematic uncertainties (described in Section 5).

The lepton momentum scale and resolution are calibrated using the dilepton mass distributions in Drell–Yan events. The detailed procedures and parameterizations of the scale and resolution corrections depend on the lepton, but the general approach is similar for the four lepton categories [57]. The corrections are applied to both the measured and simulated leptons momenta, so that the average dilepton mass values in a narrow window around the Z resonance, in various bins of kinematic variables, match the corresponding reference values, derived from the smeared momenta of post-FSR muons or dressed generated electrons (produced by combining the momenta of post-FSR electrons and nearby photons within a $\Delta R = 0.1$ cone). Also the resolution of the simulated events matches that of the data; they are first parameterized using the true lepton-momentum response distributions and then corrected by fitting the dilepton mass distributions.

4. Backgrounds

The small multijet background in the signal region is evaluated from multijet enriched control regions (CRs) in data, using transfer factors (TFs) that depend on the muon or electron $|\eta|$, p_T, and category. Four exclusive categories are considered: leptons that pass single-lepton triggers, leading and trailing leptons that pass dilepton triggers, and nontriggering leptons. To select the CRs, the following inverted lepton identification criteria are used: muons must fail the isolation criteria and electrons of all categories (central, forward ECAL, and HCAL) must fail the loose ID criteria (which has an efficiency of about 90%). Central electrons must additionally fail at least two criteria from the medium ID. As shown in Fig. 3, the data and predictions agree in the same-sign multijet CR, which validates the multijet background evaluation method.

The normalization of the EW and top quark backgrounds to the integrated luminosity uses NNLO inclusive cross sections and is validated (and the corresponding systematic uncertainties are evaluated) using μe samples selected using single-muon or single-electron triggers. The central-forward μg and μh control regions are used to validate the multijet background evaluation and derive residual $|\eta|$- and p_T-dependent scale factors to be applied to the simulated W+jets events with incorrectly identified forward electrons. The scale factors are derived in two steps: first, the inclusive transverse mass (m_T) distribution is fitted with floating multijet and W+jets contributions; then, $|\eta|$- and p_T-dependent scale factors are derived from the W+jets enriched CR, selected with an additional $m_T > 40$ GeV requirement. In the W+jets-enriched region, the multijet background estimate is scaled using the results from the first step. Fig. 4 compares the measured and simulated $\cos\theta_{CS}$ distributions, after applying the scale factors. In the CF channels with a forward HCAL electron, events with small $|\cos\theta_{CS}|$ values do not pass the acceptance cuts.

5. Systematic uncertainties

Besides the statistical uncertainties in the lepton efficiencies, we consider 31 independent sources of systematic uncertainty affecting the efficiency for central leptons, including signal shape model, background model, tag selection, pileup model, trigger prefiring probabilities, dilepton p_T model, beamspot position, as well as mass range and bin width of the dilepton mass histograms used in the tag-and-probe method. We also consider the generator-matching requirement used to make a signal template, fitting instead of counting in the determination of the trigger efficiencies, alternative background subtraction (only for electrons), alternative factorization of reconstruction times identification efficiencies (only for muons), and a residual η-dependent scaling factor that makes the simulated lepton η distribution agree with the data.

For the g and h electrons, whose efficiency measurements (especially for h) are more challenging because the signal and background dilepton mass shapes are more similar in some measurement bins, we consider fewer but more conservative systematic variations. The 9 systematic sources include the signal shape model, 3 alternative variations in the event selections to change the signal and background contributions (2 for the central tag electron, 1 for the m_T), fit range, dilepton p_T model, trigger prefiring probabilities, beamspot position, and dilepton mass window for the integral calculation.

For the multijet background, a conservative ±50% uncertainty covers the residual differences seen in the μg and μh control regions. The W+jets background shapes are obtained from simulation, but in the forward channels scale factors are applied as functions of the forward, often misidentified, electron p_T and $|\eta|$. A 25% uncertainty is estimated by varying the multijet contribution by 50% in the W+jets CR where the scale factors are evaluated. For the central-central channels, both the multijet and W+jets contributions are very small. An uncertainty of 10% is assigned to the top quark and $Z/\gamma \to \tau\tau$ background estimates, consistent with the differences observed in the μe CR. Other backgrounds have negligible uncertainties.

The statistical uncertainties in the lepton momentum corrections are evaluated by generating bootstrap replicas [58] for data and simulated samples. We consider the following systematic sources: background es-

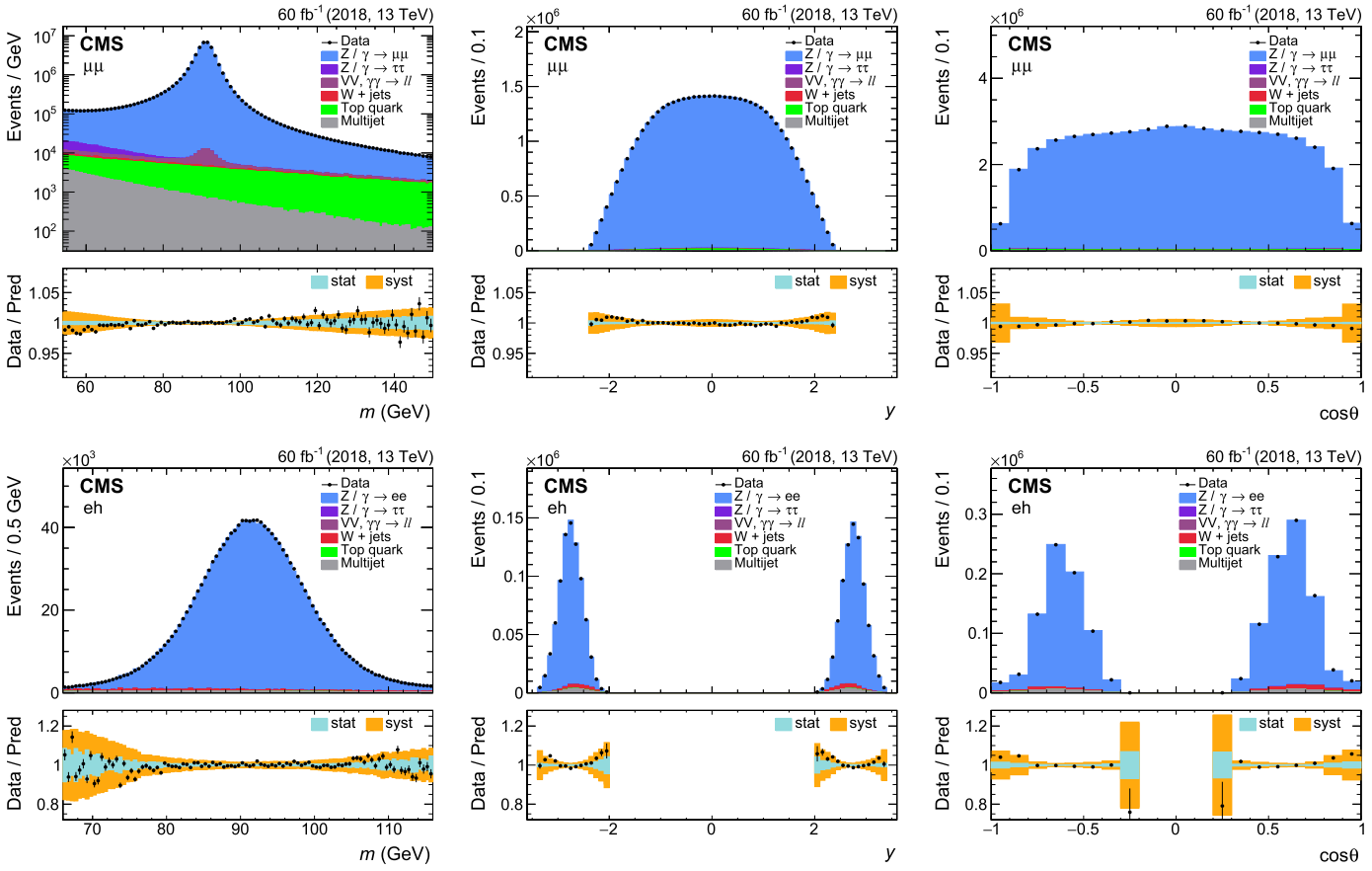

Fig. 5. Dilepton mass (left), rapidity (middle), and $\cos\theta_{\mathrm{CS}}$ (right) distributions, for the μμ (upper) and eh (lower) channels in the 2018 sample, after applying all the corrections. The signal is scaled to match the total number of events in the data.

timate, dilepton p_{T} model, mass ranges for scale and resolution corrections, a material correction bias for muons, a nonlinearity correction to the electron energy, and different parameterizations of resolution corrections for central and forward electrons.

In addition to the statistical uncertainties in the data sample used to determine the weight factors applied to the simulated samples to correct for the trigger prefiring, we consider systematic uncertainties of ±20% in each measurement $|\eta|$ bin in two ways: independent of p_{T} and linear versus $1/p_{\mathrm{T}}$ for $p_{\mathrm{T}} > 20$ GeV. We also vary the trigger prefiring probability of each object linearly with the event number in each run (i.e., approximately versus time) so that the average measured per-object trigger prefiring probability is unchanged. The ECAL trigger prefiring probabilities, measured in bins of η and p_{T}, are parameterized as functions of p_{T} in each η bin. The differences between the best fit values and the per-bin measurements are an additional systematic uncertainty.

To estimate the uncertainty associated with mismodeling of the beamspot position, we reweight the MC samples using the measured distribution of the primary vertex z position. Pileup uncertainties are estimated varying by ±5% the nominal total inelastic cross section [52] used to calculate the pileup distribution. The electron charge misidentification uncertainty is evaluated by removing from the simulation the correction to the misidentification rate.

The renormalization and factorization scales, μ_{R} and μ_{F}, are each varied independently by a factor of 2, up and down, such that their ratio remains within $0.5 < \mu_{\mathrm{R}}/\mu_{\mathrm{F}} < 2.0$. The maximum deviation among these six variants relative to the nominal choice is assigned as a systematic uncertainty associated with the missing higher-order QCD corrections and is included (in quadrature) in the theory uncertainty. The uncertainty in the modeling of the dilepton p_{T} distribution is estimated as the difference between correcting or not the simulated p_{T} distribution to match the data.

The following uncertainties, due to missing higher-order EW corrections, are considered: the treatment of finite-width effects by comparing the default complex mass (CM) scheme with the pole scheme (PS) for the propagator; and the difference between the default EW input scheme (G_{μ}, $\sin^2\theta^{\ell}_{\mathrm{eff}}$, m_{Z}) and an alternative scheme using the α_{em}, $\sin^2\theta^{\ell}_{\mathrm{eff}}$, and m_{Z} parameters. We also evaluate the effect of uncertainties in the input parameters of the default scheme, by varying G_{μ} and the masses of the Z boson and of the top quark within their uncertainties [2]. The uncertainty affecting the FSR modeling is estimated in two ways: as the difference between the PHOTOS values including or not matrix element corrections to the first emission, and as the difference between the PHOTOS and PYTHIA evaluations. Uncertainties due to the missing effects of interference between the initial and final state radiation are considered negligible.

The PDFs dominate the uncertainty of $\sin^2\theta^{\ell}_{\mathrm{eff}}$ measurements in hadron collisions because they affect the size of the dilution of the observed A_{FB} and the fraction of dileptons produced in $\mathrm{u\bar{u}}$ and $\mathrm{d\bar{d}}$ interactions. Several PDF sets, described in the next sections, are considered to evaluate the corresponding uncertainty. Using the fact that $\sin^2\theta^{\ell}_{\mathrm{eff}}$ and the PDFs affect differently the $m_{\ell\ell}$-dependence of the observed A_{FB}, the PDF uncertainties are profiled [59] while extracting $\sin^2\theta^{\ell}_{\mathrm{eff}}$. For profiling, we use the nominal tolerance criterion of $\Delta\chi^2 = 1$.

Fig. 5 compares the measured and predicted distributions of the dilepton mass, rapidity, and $\cos\theta_{\mathrm{CS}}$, using the μμ and eh channels in the 2018 data sample. The simulated and measured distributions agree within their uncertainties.

6. Measurement bins and interpretation model

We measure $\sin^2\theta^{\ell}_{\mathrm{eff}}$ in two ways: by fitting the observed weighted $A^{\mathrm{w}}_{\mathrm{FB}}(|y|, m)$ distribution and by fitting the unfolded angular coefficient

Table 2
Dilepton rapidity and mass binning used in the fits; $n_{|y|}$, n_m, and n_M are the numbers of bins in each category.

Channel	Absolute rapidity bin edges												$n_{\|y\|}$
μμ, ee	0.0	0.4	0.8	1.2	1.6	2.0	2.4						6
eg				1.2	1.6	2.0	2.4	2.7					4
eh						2.0	2.4	2.7	3.0	3.4			4
Channel	Reconstructed m bin edges (GeV)												n_m
μμ, ee	54	66	76	82	86	89.5	92.7	96	100	106	116	150	11
eg, eh		66	76	82	86	89.5	92.7	96	100	106	116		9
$\|Y\|$ range	Pre-FSR M bin edges (GeV)												n_M
0.0–1.2	54	66	76	82	86	89.5	92.7	96	100	106	116	150	11
1.2–2.4	54	66	76		86			96		106	116	150	7
2.4–3.4		66			86			96			116		3

$A_4(|Y|, M)$ of the pre-FSR dilepton system. The measurement is restricted to $|y| < 3.4$ to avoid regions where the signal acceptance is small. The mass bins in the Z region are narrow (but wider than the dimuon mass resolution), whereas elsewhere they are broad, to compensate for the smaller yields. Table 2 lists the mass and rapidity bins used in the fits.

To construct the template model used in the fits, in both methods, we use two different POWHEG event generator programs: "MiNNLO$_{PS}$" and "z_ew". The full-simulation events (about 1.4 billion, adding all data-taking periods and channels) are generated with the POWHEG MiNNLO$_{PS}$ generator. They are complemented by almost 10 billion MiNNLO$_{PS}$ generator-level events, of identical settings, to smooth the templates used in the reconstructed A_{FB}^{w} fits and in the interpretation fits, as well as by 0.3 billion events with alternative PDF weights. We also generated several samples with POWHEG-Z_ew, which provides NLO+HO weak corrections and supports a $\sin^2\theta_{eff}^{\ell}$ EW input scheme at NLO in EW [54], to construct templates for $\sin^2\theta_{eff}^{\ell}$ variations, as well as for systematic variations in the electroweak input schemes, input parameters, and alternative FSR models.

The default interpretation model is constructed by reweighting the POWHEG MiNNLO$_{PS}$ events with: (1) LO-to-NLO+HO weak correction factors, evaluated with "z_ew", that correct the cross sections and all angular coefficients in pre-FSR bins of $|Y|$, M, and P_T; (2) $|Y|$-dependent P_T weights that correct the corresponding reconstructed p_T distributions to data; and (3) smoothing weights to match the $A_4(|Y|, M, P_T)$ distribution of the large POWHEG MiNNLO$_{PS}$ sample at the generator level in full phase space. The smoothing weights greatly reduce the statistical fluctuations in pre-FSR distributions and also, to a lesser extent, in the reconstructed distributions in the smaller full simulation sample.

The FSR variations are applied using mass and rapidity distributions of the alternative FSR samples. The variations in the $\sin^2\theta_{eff}^{\ell}$, PDFs, μ_R, and μ_F input parameters are based on the corresponding samples, and per-event weights are built using the dilepton $|Y|$-M-P_T triple-differential cross sections and angular coefficients. Fig. 6 shows A_4 for different electroweak configurations and PDF sets.

All the fits described in the following sections were blinded by shifting the fitted $\sin^2\theta_{eff}^{\ell}$ by a random offset until all the systematic uncertainties were finalized and cross-checks completed.

7. Extraction of $\sin^2\theta_{eff}^{\ell}$ from A_{FB}^{w}

We extract $\sin^2\theta_{eff}^{\ell}$ by fitting the $A_{FB}^{w}(|y|, m)$ angular-weighted asymmetry to templates varying $\sin^2\theta_{eff}^{\ell}$ and PDF set, similarly to the analysis performed with the $\sqrt{s} = 8$ TeV data [14]. This method uses reconstructed variables; we use it to provide our baseline result because the positive and negative $\cos\theta_{CS}$ have approximately identical detection acceptance and efficiencies, so that their systematic uncertainties cancel to a large extent [17]. The dependence of A_{FB}^{w} on the dilepton mass con-

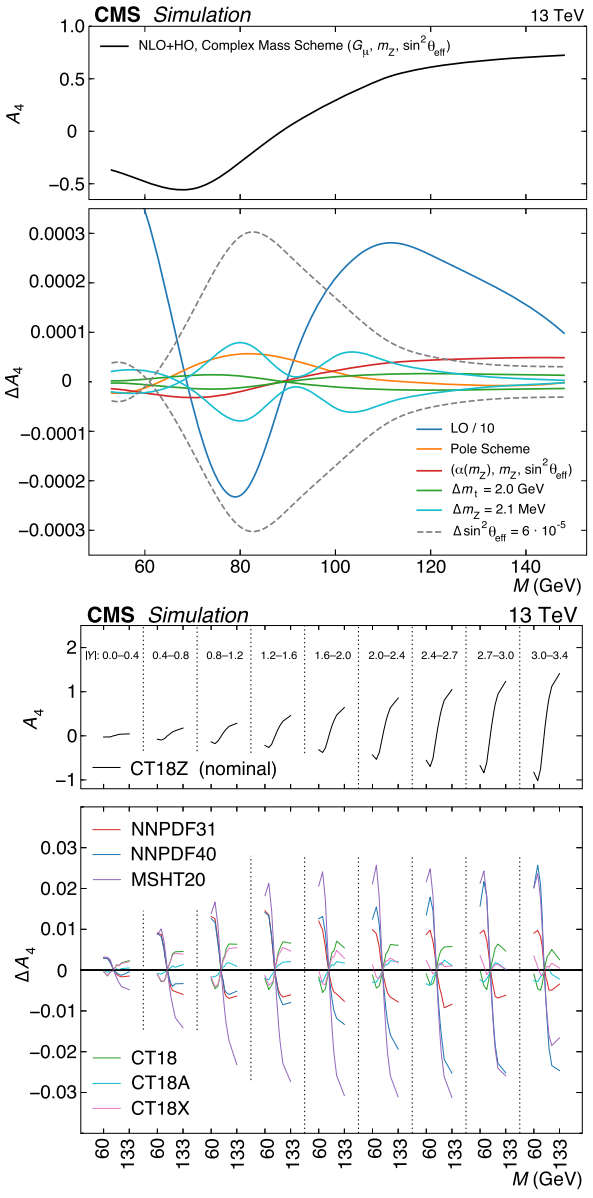

Fig. 6. The A_4 coefficient in the nominal configuration (upper panels) and its variations (lower panels) when changing the inputs mentioned in the legends: different POWHEG-Z_ew options (upper) and different PDF sets (lower). No lepton kinematic selection criteria are applied. The size of the $\sin^2\theta_{eff}^{\ell}$ variation is chosen for a clear visual demonstration.

Table 3
Free parameters in the $A_{\mathrm{FB}}^{\mathrm{W}}(|y|, m)$ fit, indicating the number of independent variations (e.g., number of rapidity bins where the uncertainties are considered uncorrelated). Some of the total values reflect the four data-taking periods and/or the four final-state channels.

Category	Parameters	Variations	Total
	$\sin^2\theta_{\mathrm{eff}}^{\ell}$	1	1
PDF	CT18Z	29	29
theo	p_{T} model (y)	9	9
theo	FSR model (μ, e)	2, 2	4
eff	Muon	31	124
eff	Central electron	31	124
eff	ECAL forward electron	9	36
eff	HCAL forward electron	9	36
calib	Muon	4	16
calib	Central electron	7	28
calib	ECAL forward electron	11	44
calib	HCAL forward electron	9	36
bkg	Multijet (y)	6, 4	80
bkg	W+jets (y)	6, 4	80
bkg	$\mathrm{Z}/\gamma \to \tau\tau$	1	16
bkg	Top quark	1	16
other	Integrated luminosity	1	4
other	Pileup	1	4
other	Charge misidentification	1	4
other	Trigger prefiring (μ, e)	4, 4	32
other	Beamspot	1	16
	Total		739

strains the PDFs while extracting $\sin^2\theta_{\mathrm{eff}}^{\ell}$ through a so-called profiling procedure [59]. As described in Ref. [17], the definition of $A_{\mathrm{FB}}^{\mathrm{W}}(|y|, m)$ depends on A_0 and, in the following, we use the simple tree-level expression for $q\overline{q}$ events, $A_0 = p_{\mathrm{T}}^2/(p_{\mathrm{T}}^2 + m^2)$. Almost identical results are obtained if we use, instead, a fixed average A_0 value in each y-m bin or an empirical A_0 parameterization based on simulated samples.

The $\sin^2\theta_{\mathrm{eff}}^{\ell}$ value is found by minimizing

$$\chi^2(s,\vec{\theta}) = |\vec{\theta}|^2 + \sum_i \left(D_i - T_i(s,\vec{\theta})\right)^T V_i^{-1} \left(D_i - T_i(s,\vec{\theta})\right),$$

where $s \equiv \sin^2\theta_{\mathrm{eff}}^{\ell}$, i represents the data-taking periods and dilepton channels, D is the measured angular-weighted $A_{\mathrm{FB}}^{\mathrm{W}}(|y|, m)$ with $n_m \times n_{|y|}$ bins, and V is the covariance matrix, which includes the statistical uncertainties in data and templates, as well as in the lepton calibration, efficiencies, and trigger prefiring probabilities. The predicted $A_{\mathrm{FB}}^{\mathrm{W}}(|y|, m)$, denoted by $T(s,\vec{\theta})$, includes background contamination and is obtained by combining all the individual differences corresponding to either s or θ_i with respect to their nominal values. Lastly, $\vec{\theta}$ is the vector of nuisance parameters, including the experimental systematic uncertainties and the PDFs. The CT18Z PDF set [47] was selected (before unblinding the analysis) to report the nominal result because it provides an accurate description of the CMS data and offers, within its uncertainties, the best coverage of the central values obtained with the other PDF sets (as will be shown later). Furthermore, this PDF set imposes identical strange quark and antiquark densities in the proton, a constraint supported by measurements of W boson production with associated charm quarks [60,61] that is not assumed in the MSHT and NNPDF sets.

The nuisance parameters are listed in Table 3, which reflects various correlations between channels and rapidity bins. The experimental systematic uncertainties are treated as uncorrelated between the different run periods, while the theoretical uncertainties are treated as correlated. Such a correlation scheme, together with the conservative treatment of experimental uncertainties per data-taking period, provides flexibility to account for possible differences in the systematic effects originating from different data-taking and reconstruction conditions. This also allows us to have a more similar correlation scheme with the unfolding procedure, described in the next section, for which decorrelations are more important to improve the fit quality (a fully identical correlation scheme for all parameters is not needed here given that $A_{\mathrm{FB}}^{\mathrm{W}}$ is much less sensitive to many systematic sources and too many free parameters add unnecessary complication since the $A_{\mathrm{FB}}^{\mathrm{W}}$ fits use numerical methods of MINUIT [62] and are relatively slow).

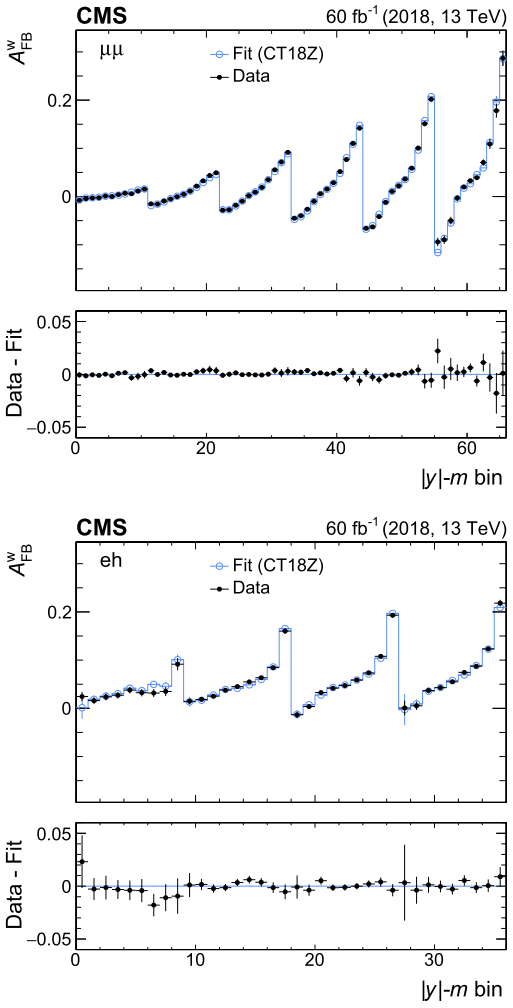

Fig. 7. Measured and best fit $\mu\mu$ (upper) and eh (lower) $A_{\mathrm{FB}}^{\mathrm{W}}(|y|, m)$ distributions for the 2018 data. The error bars represent the statistical uncertainties in the measured and simulated samples. The rapidity bins are given in Table 2.

The nominal "combined fit configuration", which includes all data-taking periods, all channels, the CT18Z PDF set, and all other nuisance parameters for systematic uncertainties, has 739 free parameters. The fit does not include, as nuisance parameters, the renormalization and factorization scale variations, nor the EW systematic uncertainty variations. Instead, individual fits are performed for each of those options and the deviations from the nominal result are considered as uncertainties. Fig. 7 shows the fitted $A_{\mathrm{FB}}^{\mathrm{W}}$ distributions for the $\mu\mu$ and eh channels, using the 2018 data sample. The agreement between the data and best-fit distributions is excellent in all channels and years. None of the nuisance parameters has a significant pull zero. The largest 14 impacts come from the nuisance parameters of PDF uncertainties, which dominate the uncertainties in this measurement.

To estimate the statistical contributions from various experimental systematic uncertainties in $\sin^2\theta_{\mathrm{eff}}^{\ell}$, we compute by how much the best fit uncertainty increases when adding the corresponding contributions to the covariance matrix of the statistical uncertainties in the data. Individual or grouped systematic uncertainties are calculated by fixing the corresponding nuisance parameter(s) to the best fit values obtained in the nominal fit and evaluating the decrease in the uncertainty: the

Table 4
Fitted $\sin^2\theta^{\ell}_{\text{eff}}$ (in units of 10^{-5}) for the four channels and their sum ($\ell\ell$), using the full data sample. The fit quality is good, as indicated by the χ^2 probabilities (p). The experimental systematic uncertainties ("exp") are the sum of the values in the five rightmost columns, corresponding to the statistical uncertainties of the MC samples and the categories listed in Table 3.

	χ^2_{min}	bins	p (%)	$\sin^2\theta^{\ell}_{\text{eff}}$	stat	exp	th	PDF	MC	bg	eff	calib	other
μμ	241	264	83	$23\,142 \pm 38$	17	17	6	30	13	3	2	5	4
ee	257	264	60	$23\,171 \pm 41$	22	18	5	30	14	4	5	3	7
eg	119	144	93	$23\,253 \pm 61$	30	40	3	44	23	11	12	20	8
eh	105	144	99	$23\,114 \pm 48$	18	33	9	37	14	10	16	18	6
$\ell\ell$	731	816	98	$23\,152 \pm 31$	10	15	8	27	8	4	6	6	3

quadratic difference from the nominal uncertainty is taken as the corresponding uncertainty. Table 4 presents the results obtained for the four channels using the full data sample, specifying the total and partial uncertainties. The largest contribution to the total theoretical uncertainty comes from the renormalization and factorization scale variations (0.00008). The four results are in agreement, as expected from lepton flavor universality. The μμ and ee channels give a combined uncertainty of 0.00034, which is reduced to 0.00031 by adding the CF channels.

8. Measurement of A_4 and extraction of $\sin^2\theta^{\ell}_{\text{eff}}$

We also extract $\sin^2\theta^{\ell}_{\text{eff}}$ through the unfolded A_4 measurements, at Born level, in the pre-FSR dilepton $|Y|$-M bins. The $A_4(|Y|, M)$ values are obtained by minimizing

$$\chi^2(\vec{p},\vec{\nu}) = |\vec{\nu}|^2 + \sum_i \left(D_i - T_i(\vec{p},\vec{\nu})\right)^T V_i^{-1} \left(D_i - T_i(\vec{p},\vec{\nu})\right),$$

where i indicates the four data-taking periods and four dilepton channels, $\vec{p}$ represents the parameters of interest, which are A_4 and the various weights (strength factors κ), $\vec{\nu}$ is the vector of all nuisance parameters of systematic uncertainties, V is the covariance matrix of statistical uncertainties, which includes the statistical uncertainties in data, signal MC simulations, backgrounds (MC simulation and CRs), efficiencies, calibration, and trigger prefiring probabilities, D is the observed numbers of data events in the $r = (|y|, m, \cos\theta_{\text{CS}})$ bins, and T is the vector of the corresponding predictions. For each sample and bin r,

$$T_r(\vec{p},\vec{\nu}) = \sum_g S^g_r(\vec{p},\vec{\nu}) + S^o_r(\vec{\kappa},\vec{\nu}) + B_r(\vec{\nu}),$$

where S^g_r is the signal contribution from the pre-FSR bin $g = (|Y|, M, C)$, with C being the pre-FSR $\cos\theta_{\text{CS}}$ bin, to the reconstructed bin r, calculated as

$$S^g_r(\kappa, A_4, A_0) = S^g_{r,0}\,\kappa\,\frac{\int_C f(x; A_4, A_0)\,\mathrm{d}x}{\int_C f(x; A_{4,0}, A_{0,0})\,\mathrm{d}x},$$

where $S^g_{r,0}$, $A_{4,0}$, and $A_{0,0}$ denote reference predictions evaluated from simulation, and

$$f(x; A_4, A_0) = 1 + x^2 + 0.5\,A_0\,(1 - 3x^2) + A_4\,x.$$

The S^o_r term represents the signal contribution from the underflow plus overflow pre-FSR bins to the reconstructed bin r. These predictions are scaled according to floating strength-factor values in the underflow and overflow measurement rapidity and mass bins. The B_r term represents the background contribution.

In each of the nine rapidity bins we have different numbers of mass bins for A_4 and A_0, shown in Table 2, driven by the dilepton mass resolutions. For the strength factors, which are more sensitive to bin migrations, we use wider (and common) mass bins for all rapidity bins. In addition, the central mass bin of each channel is used for the resolution calibration of the reconstructed leptons and, therefore, they cannot provide independent strength factor measurements in finer bins. Therefore, for the strength factors in the central-central channels, we use dilepton mass bins of edges 54, 66, 82, 100, 116, and 150 GeV, while one single bin is used for the central-forward channels: 66–116 GeV.

Table 5
Numbers of bins and free parameters used in the unfolding.

Data-taking periods:	4
Channels: μμ, ee, eg, eh	4
$\|y\|$ bins in the four channels: $6+6+4+4$	20
$\|y\|$-m bins: $2\times(6\times11)+2\times(4\times9)$	204
$\cos\theta_{\text{CS}}$ bins	20
Bins with more than 10 predicted events	14 205
$A_4(\|Y\|, M)$ parameters: $3\times(11+7+3)$	63
$\kappa(\|Y\|, M)$ parameters: $6\times5+4\times1+4\times1$	38
Nuisance parameters for syst. uncertainties	3 361

Modeling the differential distributions is more challenging than asymmetries. Therefore, we further decorrelate some of the systematic uncertainties in the unfolding to improve the best-fit χ^2. Table 5 presents the numbers of bins and free parameters involved in the unfolding. The main differences with respect to Table 3 are: (1) the multijet and W+jets background contributions are decorrelated in the measurement $|y|$ and m bins; (2) the top quark and $Z/\gamma \to \tau\tau$ backgrounds are decorrelated in the $|y|$ bins; (3) the forward electron efficiencies are decorrelated in $|\eta|$ bins; (4) the PDF and α_S uncertainties correspond to 101 eigenvectors of the hessian NNPDF31 PDF set; (5) and there are 63 additional nuisance parameters for $A_0(|Y|, M)$ with a loose prior uncertainty of 50%, which allow us to also fit them in the forward-rapidity bins. The total number of nuisance parameters is 3361. In the χ^2 calculation we only include y-m-$\cos\theta_{\text{CS}}$ bins that have a predicted content of more than 10 events. This set of bins is decided once for the default theory model and is not changed. The minimization is performed with the L-BFGS method [63], which is based on the analytic gradient calculation of the minimization function. The covariance matrix is evaluated analytically by calculating the inverse of the corresponding Hessian matrix.

Fig. 8 shows the μμ and eh $\cos\theta_{\text{CS}}$ distributions for the 2018 samples, for the Z peak and illustrative rapidity bins of the combined fit. Data in all y-m bins, dilepton channels, and years are described very well by the fit.

We extract $\sin^2\theta^{\ell}_{\text{eff}}$ from the measured $A_4(|Y|, M)$ using the corresponding templates. Adding the four channels, we have 63 A_4 measurements in $|Y|$-M bins (Table 2). In each fit, we float the $\sin^2\theta^{\ell}_{\text{eff}}$ and PDF nuisance parameters. The small EW and Z boson p_{T} modeling uncertainty is included in the covariance matrix calculation. For the μ_{R} and μ_{F} uncertainties, the fit is repeated for each of the six variations and the maximum deviation is used as uncertainty. In addition to the default result, obtained with the CT18Z PDFs, we also extract $\sin^2\theta^{\ell}_{\text{eff}}$ with other recent PDF sets. Fig. 9 shows the measured and best fit $A_4(|Y|, M)$ distributions for the full data sample. The corresponding best fit $\sin^2\theta^{\ell}_{\text{eff}}$ and χ^2 values are listed in Table 6. The results of the four dilepton channels are compatible with each other.

As a cross-check, we also extracted $\sin^2\theta^{\ell}_{\text{eff}}$ by directly fitting the observed $\cos\theta_{\text{CS}}$ distributions. The fit configuration is the same as before,

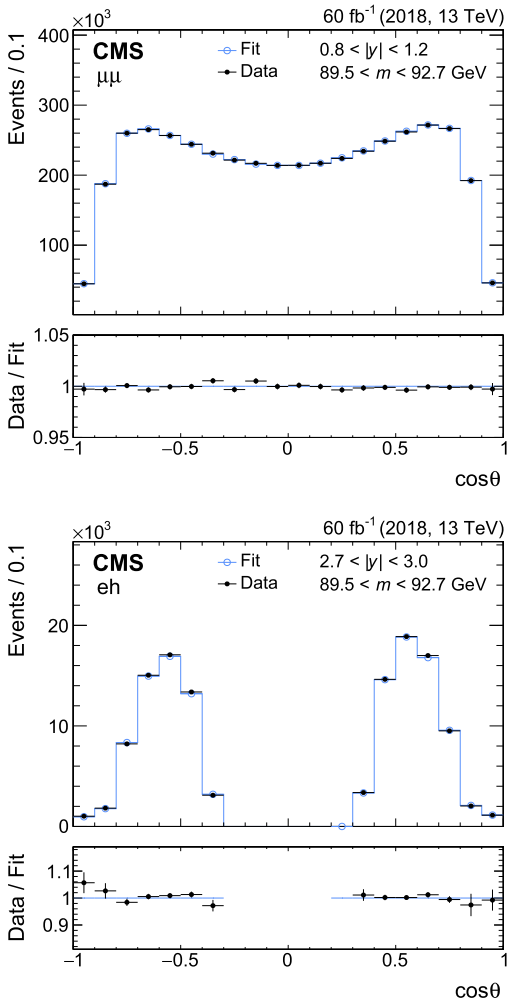

Fig. 8. Measured and best fit μμ (upper) and eh (lower) $\cos\theta_{CS}$ distributions for 2018, for the Z boson peak and two rapidity bins. The error bars represent the statistical uncertainties.

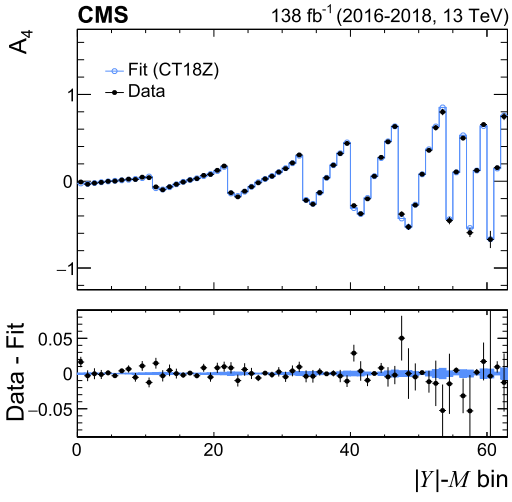

Fig. 9. Measured and best fit $A_4(|Y|, M)$ distributions for the combined 2016–2018 fit with the CT18Z PDF set. The shaded band represents the post-fit PDF uncertainty.

Table 6
Measured $\sin^2\theta^{\ell}_{\text{eff}}$ values (in units of 10^{-5}) when using the $A_4(|Y|, M)$ distributions for the four final-state channels and their sum.

Channel	χ^2_{min}	bins	p (%)	$\sin^2\theta^{\ell}_{\text{eff}}$
μμ	62	54	19	23 144 ± 39
ee	48	54	69	23 190 ± 43
eg	11	12	41	23 249 ± 60
eh	9	12	66	23 123 ± 48
$\ell\ell$	64	63	39	23 154 ± 32

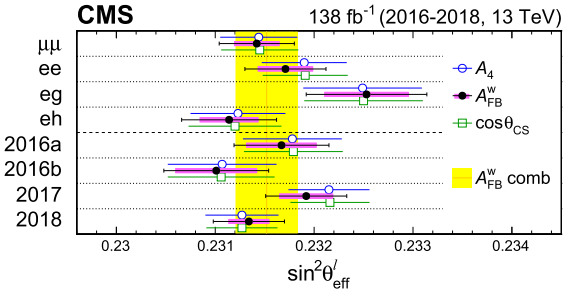

Fig. 10. Values of $\sin^2\theta^{\ell}_{\text{eff}}$ measured with the A^{w}_{FB}, A_4, and $\cos\theta_{\text{CS}}$ fits, in each of the four channels using the full 2016–2018 sample (upper) and in each of the four data-taking periods combining the four channels (lower), always with the CT18Z PDF set. The "comb" band shows the result for all channels and runs combined. For the A^{w}_{FB} results, the magenta bands show the combined statistical and experimental systematic uncertainties, and the black bars represent the total uncertainties.

except that we do it in a single fit (instead of the two-step procedure of unfolding and interpretation) by replacing the free $A_4(|Y|, M)$ parameters in the unfolding fit by the values calculated as a function of $\sin^2\theta^{\ell}_{\text{eff}}$ and PDF parameters.

9. Results

The extracted $\sin^2\theta^{\ell}_{\text{eff}}$ values are presented in Fig. 10, for the four detection channels (integrating all data) and separately for each of the four data-taking periods (combining the four channels), always using the default CT18Z PDF set. For each case, we show the measurements obtained by fitting the detector-level weighted $A^{\text{w}}_{\text{FB}}(|y|, m)$ and by fitting the unfolded $A_4(|Y|, M)$ angular coefficient of the pre-FSR dilepton; the result of the direct fitting of the measured $\cos\theta_{\text{CS}}$ distributions is also presented, as a cross-check. The statistical uncertainties in the A_4 and $\cos\theta_{\text{CS}}$ results are almost fully correlated; they are also partially correlated with those of the A^{w}_{FB} result. Small variations in the results can also be attributed to the different choices of correlations between the experimental systematic uncertainties made in the fits, as described in Section 8. The central values and uncertainties of the three methods are compatible with each other, given the correlations between samples and systematic uncertainties.

Table 7 and Fig. 11 present the $\sin^2\theta^{\ell}_{\text{eff}}$ values extracted from the measured A^{w}_{FB} or unfolded A_4 when using alternative PDF sets, combining the four detection channels and the four data-taking periods. The displayed error bars represent the total uncertainties, which include the statistical uncertainty ("stat"), and the systematic uncertainties reflecting experimental effects ("exp"), the theoretical modeling ("theo"), and the PDFs, the latter being the dominating term. In the case of our baseline result, corresponding to the A^{w}_{FB} analysis with the CT18Z PDFs, the individual uncertainties are 0.00010 (stat), 0.00015 (exp), 0.00008 (theo), and 0.00027 (PDF), leading to a total uncertainty of 0.00031, considering correlations between the various contributions.

After PDF profiling [59], all PDF sets lead to good quality fits and, without considering correlations between the PDF uncertainties, the results are compatible within uncertainties. Fig. 11 also shows the results

Table 7
Values of $\sin^2\theta^{\ell}_{\text{eff}}$ (in units of 10^{-5}) obtained by fitting the measured A^{w}_{FB} or unfolded A_4, for seven PDF sets, combining the four channels and using the full 2016–2018 sample.

PDF	A^{w}_{FB} (816 bins)		A_4 (63 bins)	
	χ^2_{min}	$\sin^2\theta^{\ell}_{\text{eff}}$	χ^2_{min}	$\sin^2\theta^{\ell}_{\text{eff}}$
NNPDF31_nnlo_as_0118_hessian [45]	725	$23\,116 \pm 29$	61	$23\,117 \pm 30$
NNPDF40_nnlo_as_01180_hessian [46]	731	$23\,128 \pm 23$	66	$23\,130 \pm 25$
MSHT20nnlo_as118 [64]	736	$23\,118 \pm 30$	76	$23\,116 \pm 32$
CT18NNLO [47]	729	$23\,165 \pm 35$	65	$23\,169 \pm 36$
CT18ZNNLO [47]	731	$23\,152 \pm 31$	64	$23\,154 \pm 32$
CT18ANNLO [47]	731	$23\,162 \pm 27$	67	$23\,165 \pm 28$
CT18XNNLO [47]	729	$23\,168 \pm 29$	64	$23\,175 \pm 30$

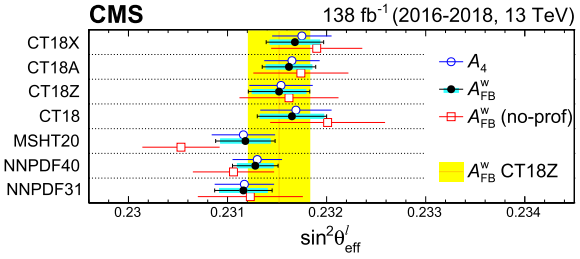

Fig. 11. Values of $\sin^2\theta^{\ell}_{\text{eff}}$ measured with the A^{w}_{FB} and A_4 fits, for seven PDF sets, combining the four channels and using the full 2016–2018 sample. The orange line and yellow band correspond to the result obtained with the CT18Z PDFs. The red open squares are the results obtained without profiling the corresponding PDF uncertainties. For the A^{w}_{FB} results, the cyan bands show the PDF uncertainties and the black bars represent the total uncertainties.

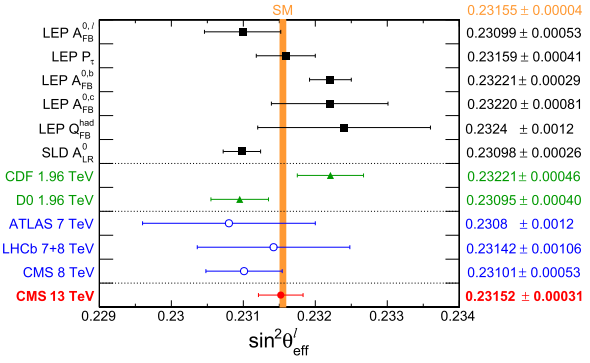

Fig. 12. Comparison of the $\sin^2\theta^{\ell}_{\text{eff}}$ values measured in this analysis with previous measurements [1,9–12,14] and the result of a SM global fit [2].

obtained without profiling the PDFs, for which the total PDF uncertainty is evaluated by adding (in quadrature) all differences obtained with each PDF error set. As a result of profiling, we see a significant reduction of the differences between the central values of the results obtained with the different PDF sets, as well as a decrease of their individual PDF uncertainties.

Fig. 12 presents the $\sin^2\theta^{\ell}_{\text{eff}}$ value measured combining the four dilepton channels and using the full 2016–2018 sample. This is the most precise result obtained at a hadron collider, to date, and agrees with the SM expectation.

In addition, the $\sin^2\theta^{\ell}_{\text{eff}}$ based on unfolded A_4 is obtained by using xFitter open-source code [65,66]. This tool facilitates the reinterpretation of the measurements in case the PDF sets or the theoretical models are updated, as well as the combination of $\sin^2\theta^{\ell}_{\text{eff}}$ values reported by different experiments.

The value of $\sin^2\theta^{\ell}_{\text{eff}}$ is determined in a profiling analysis, by minimizing the χ^2 function

Table 8
Values of $\sin^2\theta^{\ell}_{\text{eff}}$ (in units of 10^{-5}) extracted by profiling the A_4 distribution (with 63 data points) using xFitter, for several PDF sets. The reported uncertainties are the total ones, including contributions from the statistical, experimental systematic, theoretical, and PDF sources.

PDF	χ^2_{min}	$\sin^2\theta^{\ell}_{\text{eff}}$
NNPDF31_nnlo_as_0118_hessian [45]	61	$23\,117 \pm 29$
NNPDF40_nnlo_as_01180_hessian [46]	66	$23\,131 \pm 24$
MSHT20nnlo_as118 [64]	75	$23\,115 \pm 30$
CT18NNLO [47]	65	$23\,166 \pm 36$
CT18ZNNLO [47]	65	$23\,152 \pm 32$
CT18ANNLO [47]	67	$23\,164 \pm 28$
CT18XNNLO [47]	64	$23\,171 \pm 30$
MSHT20qed_an3lo [64]	69	$23\,137 \pm 31$
NNPDF40_an3lo_as_01180 [67]	65	$23\,132 \pm 25$
NNPDF40_an3lo_as_01180_mhou [68]	65	$23\,120 \pm 26$
NNPDF40_nnlo_as_01180_mhou [68]	64	$23\,110 \pm 27$
ABMP16_5_nnlo [69]	59	$23\,082 \pm 25$
PDF4LHC21_40 [70]	62	$23\,133 \pm 33$
CT18As_LatNNLO [71]	64	$23\,108 \pm 43$

$$\chi^2(\beta_{\text{exp}}, \beta_{\text{th}}) = \sum_{i=1}^{N_{\text{data}}} \frac{(\sigma_i^{\text{exp}} + \sum_j \Gamma_{ij}^{\text{exp}} \beta_{j,\text{exp}} - \sigma_i^{\text{th}} - \sum_k \Gamma_{ik}^{\text{th}} \beta_{k,\text{th}})^2}{\Delta_i^2} + \sum_j \beta_{j,\text{exp}}^2 + \sum_k \beta_{k,\text{th}}^2.$$

The correlated experimental (theoretical) uncertainties are included in the nuisance vector β_{exp} (β_{th}) and their impact on the measured distributions (theory predictions) is described by the matrix Γ^{exp} (Γ^{th}). The index i runs over all $N_{\text{data}} = 63$ data points of the ($|Y|$-M) double-differential A_4 measurement, combining the four detection channels and using the four data-taking periods, whereas the j and k indices correspond to the experimental and theoretical uncertainty nuisance parameters, respectively. The measurements and the uncorrelated experimental uncertainties are represented by σ_i^{exp} and Δ_i, respectively, whereas the theoretical predictions are denoted by σ_i^{th}. The information in the experimental covariance matrix of the double-differential A_4 measurement is included in the Γ^{exp} matrix.

The theoretical uncertainty includes contributions from the missing higher-order QCD and EW corrections, as evaluated with powheg-z_ew, and PDF uncertainties, evaluated by using grids generated at NLO with MadGraph5_aMC@NLO [50] and PineAPPL [72,73]. The matrix Γ^{th} includes nuisance parameters reflecting the missing higher-order EW corrections, the PDF Hessian uncertainties, and the $\sin^2\theta^{\ell}_{\text{eff}}$ parameter itself, which is left free in the fit.

The $\sin^2\theta^{\ell}_{\text{eff}}$ values extracted with xFitter are listed in Table 8. The first seven rows report values that can be directly compared to those shown in the rightmost columns of Table 7. We see that the two sets of values are in agreement, with small differences in the central values that are attributed to the different statistical analysis framework.

The remaining seven rows of Table 8 present values obtained with alternative PDF sets: MSHT20 [64], NNPDF40 [67,68], ABMP16 [69], PDF4LHC21 [70], and CT18As [71]. The CT18As PDF set assumes asymmetric sea strange quark densities. The NNPDF40 label "mhou" indicates that these PDFs sets include "missing higher-order uncertainties". The differences in the results obtained with the various PDF sets are mostly attributed to differences in the parametrizations and assumptions on the flavor decomposition.

Given the crucial role of the PDFs in the extraction of $\sin^2\theta^{\ell}_{\text{eff}}$ and the importance of the PDF profiling procedure in reducing the corresponding uncertainty, we performed an alternative analysis where the PDFs and $\sin^2\theta^{\ell}_{\text{eff}}$ are simultaneously extracted. Although a global PDF fit based on multiple data sets from different experiments is beyond the scope of the present study, a basic QCD fit has been performed, considering only the deep inelastic scattering data from HERA [74] and the present A_4 measurement. The xFitter framework is used and the parametrization of the HERAPDF2.0 NNLO analysis [74] is assumed, as in the profiling exercise. The fit is performed at NNLO, applying the A_4 theoretical model described above. The goodness of fit is expressed by a total χ^2/ndf of 1457/1194. The somewhat larger χ^2 of HERA data of 1394/1145, similar to the original publication [74] is observed, while the CMS A4 measurement contributes with 64/63, including correlations. The $\sin^2\theta^{\ell}_{\text{eff}}$ (both the central value and the uncertainty) is in good agreement (within 0.00002) with that obtained by profiling the HERAPDF20 set, giving confidence in the results obtained with the PDF profiling technique.

The results reported in this Letter are tabulated in the HEPData record for this analysis [75].

10. Summary

A precise measurement of the forward-backward asymmetry has been performed, using proton-proton collisions at $\sqrt{s} = 13\,\text{TeV}$ collected in 2016–2018 by the CMS experiment and corresponding to a total integrated luminosity of $138\,\text{fb}^{-1}$. The measurement is based on the study of Drell–Yan dimuon and dielectron events. The effective leptonic electroweak mixing angle $\sin^2\theta^{\ell}_{\text{eff}}$ is extracted very precisely by fitting the detector-level angular-weighted $A^{\text{w}}_{\text{FB}}(|y|, m)$ and the unfolded $A_4(|Y|, M)$ angular coefficient of the pre-FSR dilepton, obtaining compatible results. Given that the angular-weighted asymmetry method [17] benefits from the cancelation of systematic uncertainties in the detection acceptance and efficiencies, we use this method for our baseline result. This measurement has a significantly smaller uncertainty than the previous CMS result [14] because of the larger data sample, an improved analysis technique, and the inclusion of central-forward dielectron configurations. Using the CT18Z set of parton distribution functions we obtain

$$\sin^2\theta^{\ell}_{\text{eff}} = 0.23152 \pm 0.00010\,(\text{stat}) \pm 0.00015\,(\text{exp}) \pm 0.00008\,(\text{theo}) \pm 0.00027\,(\text{PDF}),$$

where "stat", "exp", "theo", and "PDF" denote, respectively, the statistical uncertainty and the systematic uncertainties reflecting experimental effects, the theory modeling, and the PDFs. Accounting for the correlations between the various contributions, the total uncertainty, dominated by the PDF term, is 0.00031. It varies between 0.00024 and 0.00035 depending on the PDF set. From the unfolded $A_4(|Y|, M)$ angular coefficient, and using the CT18Z PDF set, the extracted $\sin^2\theta^{\ell}_{\text{eff}}$ value is 0.23154 ± 0.00032 or 0.23152 ± 0.00032, depending on the analysis framework.

Our result agrees with the standard model expectation, 0.23155 ± 0.00004, and is the most precise hadron-collider measurement. The precision is comparable to that of the two most precise measurements performed in e^+e^- collisions at LEP and SLD, with respective uncertainties of 0.00029 and 0.00026. The A_4 coefficient, measured as a function of the dilepton mass and rapidity, can be used in combination with other LHC measurements or to improve the $\sin^2\theta^{\ell}_{\text{eff}}$ measurement using future PDF sets.

Declaration of competing interest

The authors declare that they have no known competing financial interests or personal relationships that could have appeared to influence the work reported in this paper.

Acknowledgements

We congratulate our colleagues in the CERN accelerator departments for the excellent performance of the LHC and thank the technical and administrative staffs at CERN and at other CMS institutes for their contributions to the success of the CMS effort. In addition, we gratefully acknowledge the computing centers and personnel of the Worldwide LHC Computing Grid and other centers for delivering so effectively the computing infrastructure essential to our analyses. Finally, we acknowledge the enduring support for the construction and operation of the LHC, the CMS detector, and the supporting computing infrastructure provided by the following funding agencies: SC (Armenia), BMBWF and FWF (Austria); FNRS and FWO (Belgium); CNPq, CAPES, FAPERJ, FAPERGS, and FAPESP (Brazil); MES and BNSF (Bulgaria); CERN; CAS, MOST, and NSFC (China); Minciencias (Colombia); MSES and CSF (Croatia); RIF (Cyprus); SENESCYT (Ecuador); ERC PRG, RVTT3 and MoER TK202 (Estonia); Academy of Finland, MEC, and HIP (Finland); CEA and CNRS/IN2P3 (France); SRNSF (Georgia); BMBF, DFG, and HGF (Germany); GSRI (Greece); NKFIH (Hungary); DAE and DST (India); IPM (Iran); SFI (Ireland); INFN (Italy); MSIP and NRF (Republic of Korea); MES (Latvia); LMTLT (Lithuania); MOE and UM (Malaysia); BUAP, CINVESTAV, CONACYT, LNS, SEP, and UASLP-FAI (Mexico); MOS (Montenegro); MBIE (New Zealand); PAEC (Pakistan); MES and NSC (Poland); FCT (Portugal); MESTD (Serbia); MCIN/AEI and PCTI (Spain); MoSTR (Sri Lanka); Swiss Funding Agencies (Switzerland); MST (Taipei); MHESI and NSTDA (Thailand); TUBITAK and TENMAK (Turkey); NASU (Ukraine); STFC (United Kingdom); DOE and NSF (USA).

Individuals have received support from the Marie-Curie program and the European Research Council and Horizon 2020 Grant, contract Nos. 675440, 724704, 752730, 758316, 765710, 824093, 101115353, 101002207, and COST Action CA16108 (European Union); the Leventis Foundation; the Alfred P. Sloan Foundation; the Alexander von Humboldt Foundation; the Science Committee, project no. 22rl-037 (Armenia); the Belgian Federal Science Policy Office; the Fonds pour la Formation à la Recherche dans l'Industrie et dans l'Agriculture (FRIA-Belgium); the F.R.S.-FNRS and FWO (Belgium) under the "Excellence of Science – EOS" – be.h project n. 30820817; the Beijing Municipal Science & Technology Commission, No. Z191100007219010 and Fundamental Research Funds for the Central Universities (China); The Ministry of Education, Youth and Sports (MEYS) of the Czech Republic; the Shota Rustaveli National Science Foundation, grant FR-22-985 (Georgia); the Deutsche Forschungsgemeinschaft (DFG), among others, under Germany's Excellence Strategy – EXC 2121 "Quantum Universe" – 390833306, and under project number 400140256 - GRK2497; the Hellenic Foundation for Research and Innovation (HFRI), Project Number 2288 (Greece); the Hungarian Academy of Sciences, the New National Excellence Program - ÚNKP, the NKFIH research grants K 131991, K 133046, K 138136, K 143460, K 143477, K 146913, K 146914, K 147048, 2020-2.2.1-ED-2021-00181, and TKP2021-NKTA-64 (Hungary); the Council of Science and Industrial Research, India; ICSC – National Research Center for High Performance Computing, Big Data and Quantum Computing and FAIR – Future Artificial Intelligence Research, funded by the NextGenerationEU program (Italy); the Latvian Council of Science; the Ministry of Education and Science, project no. 2022/WK/14, and the National Science Center, contracts Opus 2021/41/B/ST2/01369 and 2021/43/B/ST2/01552 (Poland); the

Fundação para a Ciência e a Tecnologia, grant CEECIND/01334/2018 (Portugal); the National Priorities Research Program by Qatar National Research Fund; MCIN/AEI/10.13039/501100011033, ERDF "a way of making Europe", and the Programa Estatal de Fomento de la Investigación Científica y Técnica de Excelencia María de Maeztu, grant MDM-2017-0765 and Programa Severo Ochoa del Principado de Asturias (Spain); the Chulalongkorn Academic into Its 2nd Century Project Advancement Project, and the National Science, Research and Innovation Fund via the Program Management Unit for Human Resources & Institutional Development, Research and Innovation, grant B39G670016 (Thailand); the Kavli Foundation; the Nvidia Corporation; the Super-Micro Corporation; the Welch Foundation, contract C-1845; and the Weston Havens Foundation (USA).

Data availability

Release and preservation of data used by the CMS Collaboration as the basis for publications is guided by the CMS data preservation, re-use and open access policy.

References

[1] S. Schael, et al., ALEPH, DELPHI, L3, OPAL, SLD, LEP Electroweak Working Group, SLD Electroweak Group, SLD Heavy Flavour Group, Precision electroweak measurements on the Z resonance, Phys. Rep. 427 (2006) 257, https://doi.org/10.1016/j.physrep.2005.12.006, arXiv:hep-ex/0509008.

[2] R.L. Workman, et al., Particle Data Group, Review of particle physics, PTEP 2022 (2022) 083C01, https://doi.org/10.1093/ptep/ptac097.

[3] V.M. Abazov, et al., D0, Measurement of the forward-backward charge asymmetry and extraction of $\sin^2\theta_W^{\text{eff}}$ in $p\bar{p} \to Z/\gamma^* + X \to e^+e^- + X$ events produced at $\sqrt{s} = 1.96$ TeV , Phys. Rev. Lett. 101 (2008) 191801, https://doi.org/10.1103/PhysRevLett.101.191801, arXiv:0804.3220.

[4] V.M. Abazov, et al., D0, Measurement of $\sin^2\theta_{\text{eff}}^{\ell}$ and Z-light quark couplings using the forward-backward charge asymmetry in $p\bar{p} \to Z/\gamma^* \to e^+e^-$ events with $\mathcal{L} = 5.0\,\text{fb}^{-1}$ at $\sqrt{s} = 1.96$ TeV , Phys. Rev. D 84 (2011) 012007, https://doi.org/10.1103/PhysRevD.84.012007, arXiv:1104.4590.

[5] CMS Collaboration, Measurement of the weak mixing angle with the Drell–Yan process in proton-proton collisions at the LHC, Phys. Rev. D 84 (2011) 112002, https://doi.org/10.1103/PhysRevD.84.112002, arXiv:1110.2682.

[6] T. Aaltonen, et al., CDF, Indirect measurement of $\sin^2\theta_W$ (M_W) using e^+e^- pairs in the Z-boson region with $p\bar{p}$ collisions at a center-of-momentum energy of 1.96 TeV , Phys. Rev. D 88 (2013) 072002, https://doi.org/10.1103/PhysRevD.88.072002, arXiv:1307.0770.

[7] T.A. Aaltonen, et al., CDF, Indirect measurement of $\sin^2\theta_W$ (or M_W) using $\mu^+\mu^-$ pairs from γ^*/Z bosons produced in $p\bar{p}$ collisions at a center-of-momentum energy of 1.96 TeV , Phys. Rev. D 89 (2014) 072005, https://doi.org/10.1103/PhysRevD.89.072005, arXiv:1402.2239.

[8] V.M. Abazov, et al., D0, Measurement of the effective weak mixing angle in $p\bar{p} \to Z/\gamma^* \to e^+e^-$ events, Phys. Rev. Lett. 115 (2015) 041801, https://doi.org/10.1103/PhysRevLett.115.041801, arXiv:1408.5016.

[9] ATLAS Collaboration, Measurement of the forward-backward asymmetry of electron and muon pair-production in pp collisions at $\sqrt{s} = 7$ TeV with the ATLAS detector, J. High Energy Phys. 09 (2015) 049, https://doi.org/10.1007/JHEP09(2015)049, arXiv:1503.03709.

[10] LHCb Collaboration, Measurement of the forward-backward asymmetry in $Z/\gamma^* \to \mu^+\mu^-$ decays and determination of the effective weak mixing angle, J. High Energy Phys. 11 (2015) 190, https://doi.org/10.1007/JHEP11(2015)190, arXiv:1509.07645.

[11] T.A. Aaltonen, et al., CDF, Measurement of $\sin^2\theta_{\text{eff}}^{\text{lept}}$ using e^+e^- pairs from γ^*/Z bosons produced in $p\bar{p}$ collisions at a center-of-momentum energy of 1.96 TeV , Phys. Rev. D 93 (2016) 112016, https://doi.org/10.1103/PhysRevD.93.112016, arXiv:1605.02719.

[12] V.M. Abazov, et al., D0, Measurement of the effective weak mixing angle in $p\bar{p} \to Z/\gamma^* \to \ell^+\ell^-$ events, Phys. Rev. Lett. 120 (2018) 241802, https://doi.org/10.1103/PhysRevLett.120.241802, arXiv:1710.03951.

[13] CDF and D0 collaborations, Tevatron Run II combinations of the effective leptonic electroweak mixing angle, Phys. Rev. D 97 (2018) 112007, https://doi.org/10.1103/PhysRevD.97.112007, arXiv:1801.06283.

[14] CMS Collaboration, Measurement of the weak mixing angle using the forward-backward asymmetry of Drell–Yan events in pp collisions at 8 TeV , Eur. Phys. J. C 78 (2018) 701, https://doi.org/10.1140/epjc/s10052-018-6148-7, arXiv:1806.00863.

[15] J.C. Collins, D.E. Soper, Angular distribution of dileptons in high-energy hadron collisions, Phys. Rev. D 16 (1977) 2219, https://doi.org/10.1103/PhysRevD.16.2219.

[16] P. Faccioli, C. Lourenço, Particle Polarization in High Energy Physics: an Introduction and Case Studies on Vector Particle Production at the LHC, Lecture Notes in Physics, Springer, 2022.

[17] A. Bodek, A simple event weighting technique for optimizing the measurement of the forward-backward asymmetry of Drell–Yan dilepton pairs at hadron colliders, Eur. Phys. J. C 67 (2010) 321, https://doi.org/10.1140/epjc/s10052-010-1287-5, arXiv:0911.2850.

[18] CMS Collaboration, The CMS experiment at the CERN LHC, J. Instrum. 3 (2008) S08004, https://doi.org/10.1088/1748-0221/3/08/S08004.

[19] CMS Collaboration, Development of the CMS detector for the CERN LHC Run 3, J. Instrum. 19 (2024) P05064, https://doi.org/10.1088/1748-0221/19/05/P05064, arXiv:2309.05466.

[20] CMS Collaboration, Performance of the CMS Level-1 trigger in proton-proton collisions at $\sqrt{s} = 13$ TeV , J. Instrum. 15 (2020) P10017, https://doi.org/10.1088/1748-0221/15/10/P10017, arXiv:2006.10165.

[21] CMS Collaboration, The CMS trigger system, J. Instrum. 12 (2017) P01020, https://doi.org/10.1088/1748-0221/12/01/P01020, arXiv:1609.02366.

[22] CMS Collaboration, Electron and photon reconstruction and identification with the CMS experiment at the CERN LHC, J. Instrum. 16 (2021) P05014, https://doi.org/10.1088/1748-0221/16/05/P05014, arXiv:2012.06888.

[23] CMS Collaboration, Performance of the CMS muon detector and muon reconstruction with proton-proton collisions at $\sqrt{s} = 13$ TeV , J. Instrum. 13 (2018) P06015, https://doi.org/10.1088/1748-0221/13/06/P06015, arXiv:1804.04528.

[24] CMS Collaboration, Description and performance of track and primary-vertex reconstruction with the CMS tracker, J. Instrum. 9 (2014) P10009, https://doi.org/10.1088/1748-0221/9/10/P10009, arXiv:1405.6569.

[25] CMS Collaboration, Particle-flow reconstruction and global event description with the CMS detector, J. Instrum. 12 (2017) P10003, https://doi.org/10.1088/1748-0221/12/10/P10003, arXiv:1706.04965.

[26] G. Bayatian, et al., CMS HCAL, Design, performance and calibration of the CMS forward calorimeter wedges, Eur. Phys. J. C 53 (2008) 139, https://doi.org/10.1140/epjc/s10052-007-0459-4.

[27] CMS Collaboration, Performance of reconstruction and identification of τ leptons decaying to hadrons and ν_τ in pp collisions at $\sqrt{s} = 13$ TeV , J. Instrum. 13 (2018) P10005, https://doi.org/10.1088/1748-0221/13/10/P10005, arXiv:1809.02816.

[28] CMS Collaboration, Jet energy scale and resolution in the CMS experiment in pp collisions at 8 TeV , J. Instrum. 12 (2017) P02014, https://doi.org/10.1088/1748-0221/12/02/P02014, arXiv:1607.03663.

[29] CMS Collaboration, Performance of missing transverse momentum reconstruction in proton-proton collisions at $\sqrt{s} = 13$ TeV using the CMS detector, J. Instrum. 14 (2019) P07004, https://doi.org/10.1088/1748-0221/14/07/P07004, arXiv:1903.06078.

[30] CMS Collaboration, Strategies and performance of the CMS silicon tracker alignment during LHC Run 2, Nucl. Instrum. Methods Phys. Res., Sect. A 1037 (2022) 166795, https://doi.org/10.1016/j.nima.2022.166795, arXiv:2111.08757.

[31] CMS Collaboration, Precision luminosity measurement in proton-proton collisions at $\sqrt{s} = 13$ TeV in 2015 and 2016 at CMS, Eur. Phys. J. C 81 (2021) 800, https://doi.org/10.1140/epjc/s10052-021-09538-2, arXiv:2104.01927.

[32] CMS Collaboration, CMS luminosity measurement for the 2017 data-taking period at $\sqrt{s} = 13$ TeV , CMS Physics Analysis Summary CMS-PAS-LUM-17-004, 2018, https://cds.cern.ch/record/2621960/.

[33] CMS Collaboration, CMS luminosity measurement for the 2018 data-taking period at $\sqrt{s} = 13$ TeV , CMS Physics Analysis Summary CMS-PAS-LUM-18-002, 2019, https://cds.cern.ch/record/2676164/.

[34] CMS Collaboration, Performance of the CMS muon trigger system in proton-proton collisions at $\sqrt{s} = 13$ TeV , J. Instrum. 16 (2021) P07001, https://doi.org/10.1088/1748-0221/16/07/P07001, arXiv:2102.04790.

[35] J. Therhaag, TMVA, TMVA: toolkit for multivariate data analysis, AIP Conf. Proc. 1504 (2012) 1013, https://doi.org/10.1063/1.4771869.

[36] M. Cacciari, G.P. Salam, G. Soyez, The anti-k_T jet clustering algorithm, J. High Energy Phys. 04 (2008) 063, https://doi.org/10.1088/1126-6708/2008/04/063, arXiv:0802.1189.

[37] M. Abadi, et al., TensorFlow: large-scale machine learning on heterogeneous distributed systems, https://www.tensorflow.org/, arXiv:1603.04467, 2016.

[38] S. Frixione, P. Nason, C. Oleari, Matching NLO QCD computations with parton shower simulations: the POWHEG method, J. High Energy Phys. 11 (2007) 070, https://doi.org/10.1088/1126-6708/2007/11/070, arXiv:0709.2092.

[39] S. Alioli, P. Nason, C. Oleari, E. Re, A general framework for implementing NLO calculations in shower Monte Carlo programs: the POWHEG BOX, J. High Energy Phys. 06 (2010) 043, https://doi.org/10.1007/JHEP06(2010)043, arXiv:1002.2581.

[40] P.F. Monni, P. Nason, E. Re, M. Wiesemann, G. Zanderighi, MiNNLO$_{\text{PS}}$: a new method to match NNLO QCD to parton showers, J. High Energy Phys. 05 (2020) 143, https://doi.org/10.1007/JHEP05(2020)143, arXiv:1908.06987, Erratum: https://doi.org/10.1007/JHEP02(2022)031.

[41] P.F. Monni, E. Re, M. Wiesemann, MiNNLO$_{\text{PS}}$: optimizing $2 \to 1$ hadronic processes, Eur. Phys. J. C 80 (2020) 1075, https://doi.org/10.1140/epjc/s10052-020-08658-5, arXiv:2006.04133.

[42] T. Sjöstrand, S. Ask, J.R. Christiansen, R. Corke, N. Desai, P. Ilten, S. Mrenna, S. Prestel, C.O. Rasmussen, P.Z. Skands, An introduction to PYTHIA 8.2, Comput. Phys. Commun. 191 (2015) 159, https://doi.org/10.1016/j.cpc.2015.01.024, arXiv:1410.3012.

[43] E. Barberio, Z. Wąs, PHOTOS: a universal Monte Carlo for QED radiative corrections. Version 2.0, Comput. Phys. Commun. 79 (1994) 291, https://doi.org/10.1016/0010-4655(94)90074-4.

[44] P. Golonka, Z. Wąs, PHOTOS Monte Carlo: a precision tool for QED corrections in Z and W decays, Eur. Phys. J. C 45 (2006) 97, https://doi.org/10.1140/epjc/s2005-02396-4, arXiv:hep-ph/0506026.
[45] R.D. Ball, et al., NNPDF, Parton distributions from high-precision collider data, Eur. Phys. J. C 77 (2017) 663, https://doi.org/10.1140/epjc/s10052-017-5199-5, arXiv:1706.00428.
[46] R.D. Ball, et al., NNPDF, The path to proton structure at 1% accuracy, Eur. Phys. J. C 82 (2022) 428, https://doi.org/10.1140/epjc/s10052-022-10328-7, arXiv:2109.02653.
[47] T.-J. Hou, et al., New CTEQ global analysis of quantum chromodynamics with high-precision data from the LHC, Phys. Rev. D 103 (2021) 014013, https://doi.org/10.1103/PhysRevD.103.014013, arXiv:1912.10053.
[48] S. Bailey, T. Cridge, L.A. Harland-Lang, A.D. Martin, R.S. Thorne, Parton distributions from LHC, HERA, Tevatron and fixed target data: MSHT20 PDFs, Eur. Phys. J. C 81 (2021) 341, https://doi.org/10.1140/epjc/s10052-021-09057-0, arXiv:2012.04684.
[49] J. Butterworth, et al., PDF4LHC recommendations for LHC Run II, J. Phys. G 43 (2016) 023001, https://doi.org/10.1088/0954-3899/43/2/023001, arXiv:1510.03865.
[50] J. Alwall, R. Frederix, S. Frixione, V. Hirschi, F. Maltoni, O. Mattelaer, H.S. Shao, T. Stelzer, P. Torrielli, M. Zaro, The automated computation of tree-level and next-to-leading order differential cross sections, and their matching to parton shower simulations, J. High Energy Phys. 07 (2014) 079, https://doi.org/10.1007/JHEP07(2014)079, arXiv:1405.0301.
[51] S. Agostinelli, et al., GEANT4 , GEANT4–a simulation toolkit, Nucl. Instrum. Methods Phys. Res., Sect. A 506 (2003) 250, https://doi.org/10.1016/S0168-9002(03)01368-8.
[52] CMS Collaboration, Measurement of the inelastic proton-proton cross section at $\sqrt{s} = 13\,\text{TeV}$, J. High Energy Phys. 07 (2018) 161, https://doi.org/10.1007/JHEP07(2018)161, arXiv:1802.02613.
[53] L. Barzè, G. Montagna, P. Nason, O. Nicrosini, F. Piccinini, A. Vicini, Neutral current Drell–Yan with combined QCD and electroweak corrections in the POWHEG BOX, Eur. Phys. J. C 73 (2013) 2474, https://doi.org/10.1140/epjc/s10052-013-2474-y, arXiv:1302.4606.
[54] M. Chiesa, F. Piccinini, A. Vicini, Direct determination of $\sin^2\theta^{\ell}_{\text{eff}}$ at hadron colliders, Phys. Rev. D 100 (2019) 071302, https://doi.org/10.1103/PhysRevD.100.071302, arXiv:1906.11569.
[55] M. Chiesa, C.L. Del Pio, F. Piccinini, On electroweak corrections to neutral current Drell–Yan with the POWHEG BOX, Eur. Phys. J. C 84 (2024) 539, https://doi.org/10.1140/epjc/s10052-024-12908-1, arXiv:2402.14659.
[56] CMS Collaboration, Measurement of the inclusive W and Z production cross sections in pp collisions at $\sqrt{s} = 7\,\text{TeV}$, J. High Energy Phys. 10 (2011) 132, https://doi.org/10.1007/JHEP10(2011)132, arXiv:1107.4789.
[57] A. Bodek, A. van Dyne, J.Y. Han, W. Sakumoto, A. Strelnikov, Extracting muon momentum scale corrections for hadron collider experiments, Eur. Phys. J. C 72 (2012) 2194, https://doi.org/10.1140/epjc/s10052-012-2194-8, arXiv:1208.3710.
[58] B. Efron, Bootstrap methods: another look at the jackknife, Ann. Stat. 7 (1979) 1, https://doi.org/10.1214/aos/1176344552.
[59] A. Bodek, J. Han, A. Khukhunaishvili, W. Sakumoto, Using Drell–Yan forward-backward asymmetry to reduce PDF uncertainties in the measurement of electroweak parameters, Eur. Phys. J. C 76 (2016) 115, https://doi.org/10.1140/epjc/s10052-016-3958-3, arXiv:1507.02470.
[60] CMS Collaboration, Measurement of associated production of a W boson and a charm quark in proton-proton collisions at $\sqrt{s} = 13\,\text{TeV}$, Eur. Phys. J. C 79 (2019) 269, https://doi.org/10.1140/epjc/s10052-019-6752-1, arXiv:1811.10021.
[61] CMS Collaboration, Measurement of the muon charge asymmetry in inclusive $\text{pp} \to \text{W} + X$ production at $\sqrt{s} = 7\,\text{TeV}$ and an improved determination of light parton distribution functions, Phys. Rev. D 90 (2014) 032004, https://doi.org/10.1103/PhysRevD.90.032004, arXiv:1312.6283.
[62] F. James, M. Roos, Minuit – a system for function minimization and analysis of the parameter errors and correlations, Comput. Phys. Commun. 10 (1975) 343, https://doi.org/10.1016/0010-4655(75)90039-9.
[63] D.C. Liu, J. Nocedal, On the limited memory BFGS method for large scale optimization, Math. Program. 45 (1989) 503, https://doi.org/10.1007/BF01589116.
[64] T. Cridge, L.A. Harland-Lang, R.S. Thorne, Combining QED and approximate N^3LO QCD corrections in a global PDF fit: MSHT20qed_an3lo PDFs, arXiv:2312.07665, 2023.
[65] S. Alekhin, et al., HERAFitter, Eur. Phys. J. C 75 (2015) 304, https://doi.org/10.1140/epjc/s10052-015-3480-z, arXiv:1410.4412.
[66] S. Camarda, et al., HERAFitter developers' Team, QCD analysis of W- and Z-boson production at Tevatron, Eur. Phys. J. C 75 (2015) 458, https://doi.org/10.1140/epjc/s10052-015-3655-7, arXiv:1503.05221.
[67] R.D. Ball, et al., NNPDF, The path to N^3LO parton distributions, Eur. Phys. J. C 84 (2024) 659, https://doi.org/10.1140/epjc/s10052-024-12891-7, arXiv:2402.18635.
[68] R.D. Ball, et al., NNPDF, Determination of the theory uncertainties from missing higher orders on NNLO parton distributions with percent accuracy, Eur. Phys. J. C 84 (2024) 517, https://doi.org/10.1140/epjc/s10052-024-12772-z, arXiv:2401.10319.
[69] S. Alekhin, J. Blümlein, S. Moch, R. Placakyte, Parton distribution functions, α_s, and heavy-quark masses for LHC Run II, Phys. Rev. D 96 (2017) 014011, https://doi.org/10.1103/PhysRevD.96.014011, arXiv:1701.05838.
[70] R.D. Ball, et al., PDF4LHC Working Group, The PDF4LHC21 combination of global PDF fits for the LHC Run III, J. Phys. G 49 (2022) 080501, https://doi.org/10.1088/1361-6471/ac7216, arXiv:2203.05506.
[71] T.-J. Hou, H.-W. Lin, M. Yan, C.P. Yuan, Impact of lattice strangeness asymmetry data in the CTEQ-TEA global analysis, Phys. Rev. D 107 (2023) 076018, https://doi.org/10.1103/PhysRevD.107.076018, arXiv:2211.11064.
[72] C. Schwan, PineAPPL: NLO EW corrections for PDF processes, SciPost Phys. Proc. 8 (2022) 079, https://doi.org/10.21468/SciPostPhysProc.8.079, arXiv:2108.05816.
[73] S. Carrazza, E.R. Nocera, C. Schwan, M. Zaro, PineAPPL: combining EW and QCD corrections for fast evaluation of LHC processes, J. High Energy Phys. 12 (2020) 108, https://doi.org/10.1007/JHEP12(2020)108, arXiv:2008.12789.
[74] H. Abramowicz, et al., H1, ZEUS, Combination of measurements of inclusive deep inelastic $\text{e}^{\pm}\text{p}$ scattering cross sections and QCD analysis of HERA data, Eur. Phys. J. C 75 (2015) 580, https://doi.org/10.1140/epjc/s10052-015-3710-4, arXiv:1506.06042.
[75] HEPData record for this analysis, https://doi.org/10.17182/hepdata.153661, 2024.

The CMS collaboration

A. Hayrapetyan, A. Tumasyan [1]

Yerevan Physics Institute, Yerevan, Armenia

W. Adam, J.W. Andrejkovic, T. Bergauer, S. Chatterjee, K. Damanakis, M. Dragicevic, P.S. Hussain, M. Jeitler [2], N. Krammer, A. Li, D. Liko, I. Mikulec, J. Schieck [2], R. Schöfbeck, D. Schwarz, M. Sonawane, W. Waltenberger, C.-E. Wulz [2]

Institut für Hochenergiephysik, Vienna, Austria

T. Janssen, T. Van Laer, P. Van Mechelen

Universiteit Antwerpen, Antwerpen, Belgium

N. Breugelmans, J. D'Hondt, S. Dansana, A. De Moor, M. Delcourt, F. Heyen, S. Lowette, I. Makarenko, D. Müller, S. Tavernier, M. Tytgat [3], G.P. Van Onsem, S. Van Putte, D. Vannerom

Vrije Universiteit Brussel, Brussel, Belgium

B. Bilin, B. Clerbaux, A.K. Das, G. De Lentdecker, H. Evard, L. Favart, P. Gianneios, J. Jaramillo, A. Khalilzadeh, F.A. Khan, K. Lee, M. Mahdavikhorrami, A. Malara, S. Paredes, M.A. Shahzad, L. Thomas, M. Vanden Bemden, C. Vander Velde, P. Vanlaer

Université Libre de Bruxelles, Bruxelles, Belgium

M. De Coen, D. Dobur, G. Gokbulut, Y. Hong, J. Knolle, L. Lambrecht, D. Marckx, K. Mota Amarilo, K. Skovpen, N. Van Den Bossche, J. van der Linden, L. Wezenbeek

Ghent University, Ghent, Belgium

A. Benecke, A. Bethani, G. Bruno, C. Caputo, J. De Favereau De Jeneret, C. Delaere, I.S. Donertas, A. Giammanco, A.O. Guzel, Sa. Jain, V. Lemaitre, J. Lidrych, P. Mastrapasqua, T.T. Tran, S. Wertz

Université Catholique de Louvain, Louvain-la-Neuve, Belgium

G.A. Alves, M. Alves Gallo Pereira, E. Coelho, G. Correia Silva, C. Hensel, T. Menezes De Oliveira, C. Mora Herrera [4], A. Moraes, P. Rebello Teles, M. Soeiro, A. Vilela Pereira [4]

Centro Brasileiro de Pesquisas Fisicas, Rio de Janeiro, Brazil

W.L. Aldá Júnior, M. Barroso Ferreira Filho, H. Brandao Malbouisson, W. Carvalho, J. Chinellato [5], E.M. Da Costa, G.G. Da Silveira [6], D. De Jesus Damiao, S. Fonseca De Souza, R. Gomes De Souza, T. Laux Kuhn, M. Macedo, J. Martins [7], L. Mundim, H. Nogima, J.P. Pinheiro, A. Santoro, A. Sznajder, M. Thiel

Universidade do Estado do Rio de Janeiro, Rio de Janeiro, Brazil

C.A. Bernardes [6], L. Calligaris, T.R. Fernandez Perez Tomei, E.M. Gregores, I. Maietto Silverio, P.G. Mercadante, S.F. Novaes, B. Orzari, Sandra S. Padula

Universidade Estadual Paulista, Universidade Federal do ABC, São Paulo, Brazil

A. Aleksandrov, G. Antchev, R. Hadjiiska, P. Iaydjiev, M. Misheva, M. Shopova, G. Sultanov

Institute for Nuclear Research and Nuclear Energy, Bulgarian Academy of Sciences, Sofia, Bulgaria

A. Dimitrov, L. Litov, B. Pavlov, P. Petkov, A. Petrov, E. Shumka

University of Sofia, Sofia, Bulgaria

S. Keshri, D. Laroze, S. Thakur

Instituto De Alta Investigación, Universidad de Tarapacá, Casilla 7 D, Arica, Chile

T. Cheng, T. Javaid, L. Yuan

Beihang University, Beijing, China

Z. Hu, Z. Liang, J. Liu, K. Yi [8,9]

Department of Physics, Tsinghua University, Beijing, China

G.M. Chen [10], H.S. Chen [10], M. Chen [10], F. Iemmi, C.H. Jiang, A. Kapoor [11], H. Liao, Z.-A. Liu [12], R. Sharma [13], J.N. Song [12], J. Tao, C. Wang [10], J. Wang, Z. Wang [10], H. Zhang, J. Zhao

Institute of High Energy Physics, Beijing, China

A. Agapitos, Y. Ban, S. Deng, B. Guo, C. Jiang, A. Levin, C. Li, Q. Li, Y. Mao, S. Qian, S.J. Qian, X. Qin, X. Sun, D. Wang, H. Yang, L. Zhang, Y. Zhao, C. Zhou

State Key Laboratory of Nuclear Physics and Technology, Peking University, Beijing, China

S. Yang

Guangdong Provincial Key Laboratory of Nuclear Science and Guangdong-Hong Kong Joint Laboratory of Quantum Matter, South China Normal University, Guangzhou, China

Z. You

Sun Yat-Sen University, Guangzhou, China

K. Jaffel, N. Lu

University of Science and Technology of China, Hefei, China

G. Bauer [14], B. Li, J. Zhang

Nanjing Normal University, Nanjing, China

X. Gao [15], Y. Li

Institute of Modern Physics and Key Laboratory of Nuclear Physics and Ion-beam Application (MOE) - Fudan University, Shanghai, China

Z. Lin, C. Lu, M. Xiao

Zhejiang University, Hangzhou, Zhejiang, China

C. Avila, D.A. Barbosa Trujillo, A. Cabrera, C. Florez, J. Fraga, J.A. Reyes Vega

Universidad de Los Andes, Bogota, Colombia

F. Ramirez, C. Rendón, M. Rodriguez, A.A. Ruales Barbosa, J.D. Ruiz Alvarez

Universidad de Antioquia, Medellin, Colombia

D. Giljanovic, N. Godinovic, D. Lelas, A. Sculac

University of Split, Faculty of Electrical Engineering, Mechanical Engineering and Naval Architecture, Split, Croatia

M. Kovac, A. Petkovic, T. Sculac

University of Split, Faculty of Science, Split, Croatia

P. Bargassa, V. Brigljevic, B.K. Chitroda, D. Ferencek, K. Jakovcic, A. Starodumov [16], T. Susa

Institute Rudjer Boskovic, Zagreb, Croatia

A. Attikis, K. Christoforou, A. Hadjiagapiou, C. Leonidou, J. Mousa, C. Nicolaou, L. Paizanos, F. Ptochos, P.A. Razis, H. Rykaczewski, H. Saka, A. Stepennov

University of Cyprus, Nicosia, Cyprus

M. Finger, M. Finger Jr., A. Kveton

Charles University, Prague, Czech Republic

E. Carrera Jarrin

Universidad San Francisco de Quito, Quito, Ecuador

S. Elgammal [17], S. Khalil [18], E. Salama [17,19]

Academy of Scientific Research and Technology of the Arab Republic of Egypt, Egyptian Network of High Energy Physics, Cairo, Egypt

A. Lotfy, M.A. Mahmoud

Center for High Energy Physics (CHEP-FU), Fayoum University, El-Fayoum, Egypt

K. Ehataht, M. Kadastik, T. Lange, S. Nandan, C. Nielsen, J. Pata, M. Raidal, L. Tani, C. Veelken

National Institute of Chemical Physics and Biophysics, Tallinn, Estonia

H. Kirschenmann, K. Osterberg, M. Voutilainen

Department of Physics, University of Helsinki, Helsinki, Finland

S. Bharthuar, N. Bin Norjoharuddeen, E. Brücken, F. Garcia, P. Inkaew, K.T.S. Kallonen, T. Lampén, K. Lassila-Perini, S. Lehti, T. Lindén, L. Martikainen, M. Myllymäki, M.m. Rantanen, H. Siikonen, J. Tuominiemi

Helsinki Institute of Physics, Helsinki, Finland

P. Luukka, H. Petrow

Lappeenranta-Lahti University of Technology, Lappeenranta, Finland

M. Besancon, F. Couderc, M. Dejardin, D. Denegri, J.L. Faure, F. Ferri, S. Ganjour, P. Gras, G. Hamel de Monchenault, M. Kumar, V. Lohezic, J. Malcles, F. Orlandi, L. Portales, A. Rosowsky, M.Ö. Sahin, A. Savoy-Navarro[20], P. Simkina, M. Titov, M. Tornago

IRFU, CEA, Université Paris-Saclay, Gif-sur-Yvette, France

F. Beaudette, G. Boldrini, P. Busson, A. Cappati, C. Charlot, M. Chiusi, F. Damas, O. Davignon, A. De Wit, I.T. Ehle, B.A. Fontana Santos Alves, S. Ghosh, A. Gilbert, R. Granier de Cassagnac, A. Hakimi, B. Harikrishnan, L. Kalipoliti, G. Liu, M. Nguyen, C. Ochando, R. Salerno, J.B. Sauvan, Y. Sirois, L. Urda Gómez, E. Vernazza, A. Zabi, A. Zghiche

Laboratoire Leprince-Ringuet, CNRS/IN2P3, Ecole Polytechnique, Institut Polytechnique de Paris, Palaiseau, France

J.-L. Agram[21], J. Andrea, D. Apparu, D. Bloch, J.-M. Brom, E.C. Chabert, C. Collard, S. Falke, U. Goerlach, R. Haeberle, A.-C. Le Bihan, M. Meena, O. Poncet, G. Saha, M.A. Sessini, P. Van Hove, P. Vaucelle

Université de Strasbourg, CNRS, IPHC UMR 7178, Strasbourg, France

A. Di Florio

Centre de Calcul de l'Institut National de Physique Nucleaire et de Physique des Particules, CNRS/IN2P3, Villeurbanne, France

D. Amram, S. Beauceron, B. Blancon, G. Boudoul, N. Chanon, D. Contardo, P. Depasse, C. Dozen[22], H. El Mamouni, J. Fay, S. Gascon, M. Gouzevitch, C. Greenberg, G. Grenier, B. Ille, E. Jourd'huy, I.B. Laktineh, M. Lethuillier, L. Mirabito, S. Perries, A. Purohit, M. Vander Donckt, P. Verdier, J. Xiao

Institut de Physique des 2 Infinis de Lyon (IP2I), Villeurbanne, France

I. Lomidze, T. Toriashvili[23], Z. Tsamalaidze[24]

Georgian Technical University, Tbilisi, Georgia

V. Botta, S. Consuegra Rodríguez, L. Feld, K. Klein, M. Lipinski, D. Meuser, A. Pauls, D. Pérez Adán, N. Röwert, M. Teroerde

RWTH Aachen University, I. Physikalisches Institut, Aachen, Germany

S. Diekmann, A. Dodonova, N. Eich, D. Eliseev, F. Engelke, J. Erdmann, M. Erdmann, P. Fackeldey, B. Fischer, T. Hebbeker, K. Hoepfner, F. Ivone, A. Jung, M.y. Lee, F. Mausolf, M. Merschmeyer, A. Meyer, S. Mukherjee, D. Noll, F. Nowotny, A. Pozdnyakov, Y. Rath, W. Redjeb, F. Rehm, H. Reithler, V. Sarkisovi, A. Schmidt, C. Seth, A. Sharma, J.L. Spah, A. Stein, F. Torres Da Silva De Araujo[25], S. Wiedenbeck, S. Zaleski

RWTH Aachen University, III. Physikalisches Institut A, Aachen, Germany

C. Dziwok, G. Flügge, T. Kress, A. Nowack, O. Pooth, A. Stahl, T. Ziemons, A. Zotz

RWTH Aachen University, III. Physikalisches Institut B, Aachen, Germany

H. Aarup Petersen, M. Aldaya Martin, J. Alimena, S. Amoroso, Y. An, J. Bach, S. Baxter, M. Bayatmakou, H. Becerril Gonzalez, O. Behnke, A. Belvedere, F. Blekman[26], K. Borras[27], A. Campbell, A. Cardini, C. Cheng, F. Colombina, G. Eckerlin, D. Eckstein, L.I. Estevez Banos, O. Filatov, E. Gallo[26], A. Geiser, V. Guglielmi, M. Guthoff, A. Hinzmann, L. Jeppe, B. Kaech, M. Kasemann, C. Kleinwort, R. Kogler, M. Komm, D. Krücker, W. Lange, D. Leyva Pernia, K. Lipka[28], W. Lohmann[29], F. Lorkowski, R. Mankel, I.-A. Melzer-Pellmann, M. Mendizabal Morentin, A.B. Meyer, G. Milella, K. Moral Figueroa, A. Mussgiller, L.P. Nair, J. Niedziela, A. Nürnberg, Y. Otarid, J. Park, E. Ranken, A. Raspereza, D. Rastorguev, J. Rübenach, L. Rygaard, A. Saggio, M. Scham[30,27], S. Schnake[27], P. Schütze, C. Schwanenberger[26], D. Selivanova, K. Sharko, M. Shchedrolosiev, X. Shen, D. Stafford, F. Vazzoler, A. Ventura Barroso, R. Walsh, D. Wang, Q. Wang, Y. Wen, K. Wichmann, L. Wiens[27], C. Wissing, Y. Yang, A. Zimermmane Castro Santos

Deutsches Elektronen-Synchrotron, Hamburg, Germany

A. Albrecht, S. Albrecht, M. Antonello, S. Bein, L. Benato, S. Bollweg, M. Bonanomi, P. Connor, K. El Morabit, Y. Fischer, E. Garutti, A. Grohsjean, J. Haller, H.R. Jabusch, G. Kasieczka, P. Keicher, R. Klanner, W. Korcari, T. Kramer, C.c. Kuo, V. Kutzner, F. Labe, J. Lange, A. Lobanov, C. Matthies, L. Moureaux, M. Mrowietz, A. Nigamova, Y. Nissan, A. Paasch, K.J. Pena Rodriguez, T. Quadfasel, B. Raciti, M. Rieger, D. Savoiu, J. Schindler, P. Schleper, M. Schröder, J. Schwandt, M. Sommerhalder, H. Stadie, G. Steinbrück, A. Tews, M. Wolf

University of Hamburg, Hamburg, Germany

S. Brommer, M. Burkart, E. Butz, T. Chwalek, A. Dierlamm, A. Droll, U. Elicabuk, N. Faltermann, M. Giffels, A. Gottmann, F. Hartmann[31], R. Hofsaess, M. Horzela, U. Husemann, J. Kieseler, M. Klute, R. Koppenhöfer, J.M. Lawhorn, M. Link, A. Lintuluoto, S. Maier, S. Mitra, M. Mormile, Th. Müller, M. Neukum, M. Oh, E. Pfeffer, M. Presilla, G. Quast, K. Rabbertz, B. Regnery, N. Shadskiy, I. Shvetsov, H.J. Simonis, L. Sowa, L. Stockmeier, K. Tauqeer, M. Toms, N. Trevisani, R.F. Von Cube, M. Wassmer, S. Wieland, F. Wittig, R. Wolf, X. Zuo

Karlsruher Institut fuer Technologie, Karlsruhe, Germany

G. Anagnostou, G. Daskalakis, A. Kyriakis, A. Papadopoulos[31], A. Stakia

Institute of Nuclear and Particle Physics (INPP), NCSR Demokritos, Aghia Paraskevi, Greece

P. Kontaxakis, G. Melachroinos, Z. Painesis, I. Papavergou, I. Paraskevas, N. Saoulidou, K. Theofilatos, E. Tziaferi, K. Vellidis, I. Zisopoulos

National and Kapodistrian University of Athens, Athens, Greece

G. Bakas, T. Chatzistavrou, G. Karapostoli, K. Kousouris, I. Papakrivopoulos, E. Siamarkou, G. Tsipolitis, A. Zacharopoulou

National Technical University of Athens, Athens, Greece

K. Adamidis, I. Bestintzanos, I. Evangelou, C. Foudas, C. Kamtsikis, P. Katsoulis, P. Kokkas, P.G. Kosmoglou Kioseoglou, N. Manthos, I. Papadopoulos, J. Strologas

University of Ioánnina, Ioánnina, Greece

C. Hajdu, D. Horvath[32,33], K. Márton, A.J. Rádl[34], F. Sikler, V. Veszpremi

HUN-REN Wigner Research Centre for Physics, Budapest, Hungary

M. Csanád, K. Farkas, A. Fehérkuti[35], M.M.A. Gadallah[36], Á. Kadlecsik, P. Major, G. Pásztor, G.I. Veres

MTA-ELTE Lendület CMS Particle and Nuclear Physics Group, Eötvös Loránd University, Budapest, Hungary

B. Ujvari, G. Zilizi

Faculty of Informatics, University of Debrecen, Debrecen, Hungary

G. Bencze, S. Czellar, J. Molnar, Z. Szillasi

HUN-REN ATOMKI - Institute of Nuclear Research, Debrecen, Hungary

T. Novak

Karoly Robert Campus, MATE Institute of Technology, Gyongyos, Hungary

S. Bansal, S.B. Beri, V. Bhatnagar, G. Chaudhary, S. Chauhan, N. Dhingra[37], A. Kaur, A. Kaur, H. Kaur, M. Kaur, S. Kumar, K. Sandeep, T. Sheokand, J.B. Singh, A. Singla

Panjab University, Chandigarh, India

A. Ahmed, A. Bhardwaj, A. Chhetri, B.C. Choudhary, A. Kumar, A. Kumar, M. Naimuddin, K. Ranjan, M.K. Saini, S. Saumya

University of Delhi, Delhi, India

S. Baradia, S. Barman[38], S. Bhattacharya, S. Das Gupta, S. Dutta, S. Dutta, S. Sarkar

Saha Institute of Nuclear Physics, HBNI, Kolkata, India

M.M. Ameen, P.K. Behera, S.C. Behera, S. Chatterjee, G. Dash, P. Jana, P. Kalbhor, S. Kamble, J.R. Komaragiri[39], D. Kumar[39], B. Parida, P.R. Pujahari, N.R. Saha, A. Sharma, A.K. Sikdar, R.K. Singh, P. Verma, S. Verma, A. Vijay

Indian Institute of Technology Madras, Madras, India

S. Dugad, G.B. Mohanty, M. Shelake, P. Suryadevara

Tata Institute of Fundamental Research-A, Mumbai, India

A. Bala, S. Banerjee, R.M. Chatterjee, M. Guchait, Sh. Jain, A. Jaiswal, S. Kumar, G. Majumder, K. Mazumdar, S. Parolia, A. Thachayath

Tata Institute of Fundamental Research-B, Mumbai, India

S. Bahinipati[40], C. Kar, D. Maity[41], P. Mal, T. Mishra, V.K. Muraleedharan Nair Bindhu[41], K. Naskar[41], A. Nayak[41], S. Nayak, K. Pal, P. Sadangi, S.K. Swain, S. Varghese[41], D. Vats[41]

National Institute of Science Education and Research, An OCC of Homi Bhabha National Institute, Bhubaneswar, Odisha, India

S. Acharya[42], A. Alpana, S. Dube, B. Gomber[42], P. Hazarika, B. Kansal, A. Laha, B. Sahu[42], S. Sharma, K.Y. Vaish

Indian Institute of Science Education and Research (IISER), Pune, India

H. Bakhshiansohi[43], A. Jafari[44], M. Zeinali[45]

Isfahan University of Technology, Isfahan, Iran

S. Bashiri, S. Chenarani[46], S.M. Etesami, Y. Hosseini, M. Khakzad, E. Khazaie[47], M. Mohammadi Najafabadi, S. Tizchang[48]

Institute for Research in Fundamental Sciences (IPM), Tehran, Iran

M. Felcini, M. Grunewald

University College Dublin, Dublin, Ireland

M. Abbrescia [a,b], A. Colaleo [a,b], D. Creanza [a,c], B. D'Anzi [a,b], N. De Filippis [a,c], M. De Palma [a,b], W. Elmetenawee [a,b,49], L. Fiore [a], G. Iaselli [a,c], L. Longo [a], M. Louka [a,b], G. Maggi [a,c], M. Maggi [a], I. Margjeka [a], V. Mastrapasqua [a,b], S. My [a,b], S. Nuzzo [a,b], A. Pellecchia [a,b], A. Pompili [a,b], G. Pugliese [a,c], R. Radogna [a,b], D. Ramos [a], A. Ranieri [a], L. Silvestris [a], F.M. Simone [a,c], Ü. Sözbilir [a], A. Stamerra [a,b], D. Troiano [a,b], R. Venditti [a,b], P. Verwilligen [a], A. Zaza [a,b]

[a] INFN Sezione di Bari, Bari, Italy
[b] Università di Bari, Bari, Italy
[c] Politecnico di Bari, Bari, Italy

G. Abbiendi [a], C. Battilana [a,b], D. Bonacorsi [a,b], P. Capiluppi [a,b], A. Castro [a,b,†], F.R. Cavallo [a], M. Cuffiani [a,b], G.M. Dallavalle [a], T. Diotalevi [a,b], F. Fabbri [a], A. Fanfani [a,b], D. Fasanella [a], P. Giacomelli [a], L. Giommi [a,b], C. Grandi [a], L. Guiducci [a,b], S. Lo Meo [a,50], M. Lorusso [a,b], L. Lunerti [a], S. Marcellini [a], G. Masetti [a], F.L. Navarria [a,b], G. Paggi [a,b], A. Perrotta [a], F. Primavera [a,b], A.M. Rossi [a,b], S. Rossi Tisbeni [a,b], T. Rovelli [a,b], G.P. Siroli [a,b]

[a] INFN Sezione di Bologna, Bologna, Italy
[b] Università di Bologna, Bologna, Italy

S. Costa [a,b,51], A. Di Mattia [a], A. Lapertosa [a], R. Potenza [a,b], A. Tricomi [a,b,51], C. Tuve [a,b]

[a] INFN Sezione di Catania, Catania, Italy
[b] Università di Catania, Catania, Italy

P. Assiouras [a], G. Barbagli [a], G. Bardelli [a,b], B. Camaiani [a,b], A. Cassese [a], R. Ceccarelli [a], V. Ciulli [a,b], C. Civinini [a], R. D'Alessandro [a,b], E. Focardi [a,b], T. Kello [a], G. Latino [a,b], P. Lenzi [a,b], M. Lizzo [a], M. Meschini [a], S. Paoletti [a], A. Papanastassiou [a,b], G. Sguazzoni [a], L. Viliani [a]

[a] INFN Sezione di Firenze, Firenze, Italy
[b] Università di Firenze, Firenze, Italy

L. Benussi, S. Bianco, S. Meola [52], D. Piccolo

INFN Laboratori Nazionali di Frascati, Frascati, Italy

P. Chatagnon [a], F. Ferro [a], E. Robutti [a], S. Tosi [a,b]

[a] INFN Sezione di Genova, Genova, Italy
[b] Università di Genova, Genova, Italy

A. Benaglia [a], F. Brivio [a], F. Cetorelli [a,b], F. De Guio [a,b], M.E. Dinardo [a,b], P. Dini [a], S. Gennai [a], R. Gerosa [a,b], A. Ghezzi [a,b], P. Govoni [a,b], L. Guzzi [a], M.T. Lucchini [a,b], M. Malberti [a], S. Malvezzi [a], A. Massironi [a], D. Menasce [a], L. Moroni [a], M. Paganoni [a,b], S. Palluotto [a,b], D. Pedrini [a], A. Perego [a,b], B.S. Pinolini [a], G. Pizzati [a,b], S. Ragazzi [a,b], T. Tabarelli de Fatis [a,b]

[a] INFN Sezione di Milano-Bicocca, Milano, Italy
[b] Università di Milano-Bicocca, Milano, Italy

S. Buontempo [a], A. Cagnotta [a,b], F. Carnevali [a,b], N. Cavallo [a,c], F. Fabozzi [a,c], A.O.M. Iorio [a,b], L. Lista [a,b,53], P. Paolucci [a,31], B. Rossi [a]

[a] INFN Sezione di Napoli, Napoli, Italy
[b] Università di Napoli 'Federico II', Napoli, Italy
[c] Università della Basilicata, Potenza, Italy
[d] Scuola Superiore Meridionale (SSM), Napoli, Italy

R. Ardino [a], P. Azzi [a], N. Bacchetta [a,54], A. Bergnoli [a], D. Bisello [a,b], P. Bortignon [a], G. Bortolato [a,b], A. Bragagnolo [a,b], A.C.M. Bulla [a], R. Carlin [a,b], P. Checchia [a], T. Dorigo [a], F. Gasparini [a,b], U. Gasparini [a,b], S. Giorgetti [a], E. Lusiani [a], M. Margoni [a,b], A.T. Meneguzzo [a,b], M. Migliorini [a,b], J. Pazzini [a,b], P. Ronchese [a,b], R. Rossin [a,b], F. Simonetto [a,b], M. Tosi [a,b], A. Triossi [a,b], S. Ventura [a], M. Zanetti [a,b], P. Zotto [a,b], A. Zucchetta [a,b]

[a] INFN Sezione di Padova, Padova, Italy
[b] Università di Padova, Padova, Italy
[c] Università di Trento, Trento, Italy

C. Aimè [a,], A. Braghieri [a,], S. Calzaferri [a,], D. Fiorina [a,], P. Montagna [a,b,], V. Re [a,], C. Riccardi [a,b,], P. Salvini [a,], I. Vai [a,b,], P. Vitulo [a,b,]

[a] INFN Sezione di Pavia, Pavia, Italy
[b] Università di Pavia, Pavia, Italy

S. Ajmal [a,b,], M.E. Ascioti [a,b], G.M. Bilei [a,], C. Carrivale [a,b], D. Ciangottini [a,b,], L. Fanò [a,b,], M. Magherini [a,b,], V. Mariani [a,b,], M. Menichelli [a,], F. Moscatelli [a,,55], A. Rossi [a,b,], A. Santocchia [a,b,], D. Spiga [a,], T. Tedeschi [a,b,]

[a] INFN Sezione di Perugia, Perugia, Italy
[b] Università di Perugia, Perugia, Italy

C.A. Alexe [a,c,], P. Asenov [a,b,], P. Azzurri [a,], G. Bagliesi [a,], R. Bhattacharya [a,], L. Bianchini [a,b,], T. Boccali [a,], E. Bossini [a,], D. Bruschini [a,c,], R. Castaldi [a,], M.A. Ciocci [a,b,], M. Cipriani [a,b,], V. D'Amante [a,d,], R. Dell'Orso [a,], S. Donato [a,], A. Giassi [a,], F. Ligabue [a,c,], A.C. Marini [a,], D. Matos Figueiredo [a,], A. Messineo [a,b,], S. Mishra [a,], M. Musich [a,b,], F. Palla [a,], A. Rizzi [a,b,], G. Rolandi [a,c,], S. Roy Chowdhury [a,], T. Sarkar [a,], A. Scribano [a,], P. Spagnolo [a,], R. Tenchini [a,], G. Tonelli [a,b,], N. Turini [a,d,], F. Vaselli [a,c,], A. Venturi [a,], P.G. Verdini [a,]

[a] INFN Sezione di Pisa, Pisa, Italy
[b] Università di Pisa, Pisa, Italy
[c] Scuola Normale Superiore di Pisa, Pisa, Italy
[d] Università di Siena, Siena, Italy

C. Baldenegro Barrera [a,b,], P. Barria [a,], C. Basile [a,b,], F. Cavallari [a,], L. Cunqueiro Mendez [a,b,], D. Del Re [a,b,], E. Di Marco [a,b,], M. Diemoz [a,], F. Errico [a,b,], E. Longo [a,b,], J. Mijuskovic [a,b,], G. Organtini [a,b,], F. Pandolfi [a,], R. Paramatti [a,b,], C. Quaranta [a,b,], S. Rahatlou [a,b,], C. Rovelli [a,], F. Santanastasio [a,b,], L. Soffi [a,]

[a] INFN Sezione di Roma, Roma, Italy
[b] Sapienza Università di Roma, Roma, Italy

N. Amapane [a,b,], R. Arcidiacono [a,c,], S. Argiro [a,b,], M. Arneodo [a,c,], N. Bartosik [a,], R. Bellan [a,b,], A. Bellora [a,b,], C. Biino [a,], C. Borca [a,b,], N. Cartiglia [a,], M. Costa [a,b,], R. Covarelli [a,b,], N. Demaria [a,], L. Finco [a,], M. Grippo [a,b,], B. Kiani [a,b,], F. Legger [a,], F. Luongo [a,b,], C. Mariotti [a,], L. Markovic [a,b,], S. Maselli [a,], A. Mecca [a,b,], L. Menzio [a,b], P. Meridiani [a,], E. Migliore [a,b,], M. Monteno [a,], R. Mulargia [a,], M.M. Obertino [a,b,], G. Ortona [a,], L. Pacher [a,b,], N. Pastrone [a,], M. Pelliccioni [a,], M. Ruspa [a,c,], F. Siviero [a,b,], V. Sola [a,b,], A. Solano [a,b,], A. Staiano [a,], C. Tarricone [a,b,], D. Trocino [a,], G. Umoret [a,b,], R. White [a,b,]

[a] INFN Sezione di Torino, Torino, Italy
[b] Università di Torino, Torino, Italy
[c] Università del Piemonte Orientale, Novara, Italy

J. Babbar [a,b,], S. Belforte [a,], V. Candelise [a,b,], M. Casarsa [a,], F. Cossutti [a,], K. De Leo [a,], G. Della Ricca [a,b,]

[a] INFN Sezione di Trieste, Trieste, Italy
[b] Università di Trieste, Trieste, Italy

S. Dogra, J. Hong, B. Kim, J. Kim, D. Lee, H. Lee, S.W. Lee, C.S. Moon, Y.D. Oh, M.S. Ryu, S. Sekmen, B. Tae, Y.C. Yang

Kyungpook National University, Daegu, Korea

M.S. Kim

Department of Mathematics and Physics - GWNU, Gangneung, Korea

G. Bak, P. Gwak, H. Kim, D.H. Moon

Chonnam National University, Institute for Universe and Elementary Particles, Kwangju, Korea

E. Asilar, J. Choi, D. Kim, T.J. Kim, J.A. Merlin, Y. Ryou

Hanyang University, Seoul, Korea

S. Choi, S. Han, B. Hong, K. Lee, K.S. Lee, S. Lee, J. Yoo

Korea University, Seoul, Korea

J. Goh, S. Yang

Kyung Hee University, Department of Physics, Seoul, Korea

H.S. Kim, Y. Kim, S. Lee

Sejong University, Seoul, Korea

J. Almond, J.H. Bhyun, J. Choi, J. Choi, W. Jun, J. Kim, Y.W. Kim, S. Ko, H. Kwon, H. Lee, J. Lee, J. Lee, B.H. Oh, S.B. Oh, H. Seo, U.K. Yang, I. Yoon

Seoul National University, Seoul, Korea

W. Jang, D.Y. Kang, Y. Kang, S. Kim, B. Ko, J.S.H. Lee, Y. Lee, I.C. Park, Y. Roh, I.J. Watson

University of Seoul, Seoul, Korea

S. Ha, H.D. Yoo

Yonsei University, Department of Physics, Seoul, Korea

M. Choi, M.R. Kim, H. Lee, Y. Lee, I. Yu

Sungkyunkwan University, Suwon, Korea

T. Beyrouthy, Y. Gharbia

College of Engineering and Technology, American University of the Middle East (AUM), Dasman, Kuwait

F. Alazemi

Kuwait University - College of Science - Department of Physics, Safat, Kuwait

K. Dreimanis, A. Gaile, C. Munoz Diaz, D. Osite, G. Pikurs, A. Potrebko, M. Seidel, D. Sidiropoulos Kontos

Riga Technical University, Riga, Latvia

N.R. Strautnieks

University of Latvia (LU), Riga, Latvia

M. Ambrozas, A. Juodagalvis, A. Rinkevicius, G. Tamulaitis

Vilnius University, Vilnius, Lithuania

I. Yusuff[56], Z. Zolkapli

National Centre for Particle Physics, Universiti Malaya, Kuala Lumpur, Malaysia

J.F. Benitez, A. Castaneda Hernandez, H.A. Encinas Acosta, L.G. Gallegos Maríñez, M. León Coello, J.A. Murillo Quijada, A. Sehrawat, L. Valencia Palomo

Universidad de Sonora (UNISON), Hermosillo, Mexico

G. Ayala, H. Castilla-Valdez, H. Crotte Ledesma, E. De La Cruz-Burelo, I. Heredia-De La Cruz[57], R. Lopez-Fernandez, J. Mejia Guisao, C.A. Mondragon Herrera, A. Sánchez Hernández

Centro de Investigacion y de Estudios Avanzados del IPN, Mexico City, Mexico

C. Oropeza Barrera, D.L. Ramirez Guadarrama, M. Ramírez García

Universidad Iberoamericana, Mexico City, Mexico

I. Bautista, I. Pedraza, H.A. Salazar Ibarguen, C. Uribe Estrada

Benemerita Universidad Autonoma de Puebla, Puebla, Mexico

I. Bubanja, N. Raicevic

University of Montenegro, Podgorica, Montenegro

P.H. Butler

University of Canterbury, Christchurch, New Zealand

A. Ahmad, M.I. Asghar, A. Awais, M.I.M. Awan, H.R. Hoorani, W.A. Khan

National Centre for Physics, Quaid-I-Azam University, Islamabad, Pakistan

V. Avati, L. Grzanka, M. Malawski

AGH University of Krakow, Faculty of Computer Science, Electronics and Telecommunications, Krakow, Poland

H. Bialkowska, M. Bluj, M. Górski, M. Kazana, M. Szleper, P. Zalewski

National Centre for Nuclear Research, Swierk, Poland

K. Bunkowski, K. Doroba, A. Kalinowski, M. Konecki, J. Krolikowski, A. Muhammad

Institute of Experimental Physics, Faculty of Physics, University of Warsaw, Warsaw, Poland

K. Pozniak, W. Zabolotny

Warsaw University of Technology, Warsaw, Poland

M. Araujo, D. Bastos, C. Beirão Da Cruz E Silva, A. Boletti, M. Bozzo, T. Camporesi, G. Da Molin, P. Faccioli, M. Gallinaro, J. Hollar, N. Leonardo, G.B. Marozzo, T. Niknejad, A. Petrilli, M. Pisano, J. Seixas, J. Varela, J.W. Wulff

Laboratório de Instrumentação e Física Experimental de Partículas, Lisboa, Portugal

P. Adzic, P. Milenovic

Faculty of Physics, University of Belgrade, Belgrade, Serbia

D. Devetak, M. Dordevic, J. Milosevic, V. Rekovic

VINCA Institute of Nuclear Sciences, University of Belgrade, Belgrade, Serbia

J. Alcaraz Maestre, Cristina F. Bedoya, J.A. Brochero Cifuentes, Oliver M. Carretero, M. Cepeda, M. Cerrada, N. Colino, B. De La Cruz, A. Delgado Peris, A. Escalante Del Valle, D. Fernández Del Val, J.P. Fernández Ramos, J. Flix, M.C. Fouz, O. Gonzalez Lopez, S. Goy Lopez, J.M. Hernandez, M.I. Josa, J. Llorente Merino, E. Martin Viscasillas, D. Moran, C.M. Morcillo Perez, Á. Navarro Tobar, C. Perez Dengra, A. Pérez-Calero Yzquierdo, J. Puerta Pelayo, I. Redondo, S. Sánchez Navas, J. Sastre, J. Vazquez Escobar

Centro de Investigaciones Energéticas Medioambientales y Tecnológicas (CIEMAT), Madrid, Spain

J.F. de Trocóniz

Universidad Autónoma de Madrid, Madrid, Spain

B. Alvarez Gonzalez, J. Cuevas, J. Fernandez Menendez, S. Folgueras, I. Gonzalez Caballero, J.R. González Fernández, P. Leguina, E. Palencia Cortezon, J. Prado Pico, C. Ramón Álvarez, V. Rodríguez Bouza, A. Soto Rodríguez, A. Trapote, C. Vico Villalba, P. Vischia

Universidad de Oviedo, Instituto Universitario de Ciencias y Tecnologías Espaciales de Asturias (ICTEA), Oviedo, Spain

S. Bhowmik, S. Blanco Fernández, I.J. Cabrillo, A. Calderon, J. Duarte Campderros, M. Fernandez, G. Gomez, C. Lasaosa García, R. Lopez Ruiz, C. Martinez Rivero, P. Martinez Ruiz del Arbol, F. Matorras, P. Matorras Cuevas, E. Navarrete Ramos, J. Piedra Gomez, L. Scodellaro, I. Vila, J.M. Vizan Garcia

Instituto de Física de Cantabria (IFCA), CSIC-Universidad de Cantabria, Santander, Spain

B. Kailasapathy[58], D.D.C. Wickramarathna

University of Colombo, Colombo, Sri Lanka

W.G.D. Dharmaratna[59], K. Liyanage, N. Perera

University of Ruhuna, Department of Physics, Matara, Sri Lanka

D. Abbaneo, C. Amendola, E. Auffray, G. Auzinger, J. Baechler, D. Barney, A. Bermúdez Martínez, M. Bianco, A.A. Bin Anuar, A. Bocci, L. Borgonovi, C. Botta, E. Brondolin, C. Caillol, G. Cerminara, N. Chernyavskaya, D. d'Enterria, A. Dabrowski, A. David, A. De Roeck, M.M. Defranchis, M. Deile, M. Dobson, G. Franzoni, W. Funk, S. Giani, D. Gigi, K. Gill, F. Glege, J. Hegeman, J.K. Heikkilä, B. Huber, V. Innocente, T. James, P. Janot, O. Kaluzinska, O. Karacheban[29], S. Laurila, P. Lecoq, E. Leutgeb, C. Lourenço, L. Malgeri, M. Mannelli, M. Matthewman, A. Mehta, F. Meijers, S. Mersi, E. Meschi, V. Milosevic, F. Monti, F. Moortgat, M. Mulders, I. Neutelings, S. Orfanelli, F. Pantaleo, G. Petrucciani, A. Pfeiffer, M. Pierini, H. Qu, D. Rabady, B. Ribeiro Lopes, M. Rovere, H. Sakulin, S. Sanchez Cruz, S. Scarfi, C. Schwick, M. Selvaggi, A. Sharma, K. Shchelina, P. Silva, P. Sphicas[60], A.G. Stahl Leiton, A. Steen, S. Summers, D. Treille, P. Tropea, D. Walter, J. Wanczyk[61], J. Wang, K.A. Wozniak[62], S. Wuchterl, P. Zehetner, P. Zejdl, W.D. Zeuner

CERN, European Organization for Nuclear Research, Geneva, Switzerland

T. Bevilacqua[63], L. Caminada[63], A. Ebrahimi, W. Erdmann, R. Horisberger, Q. Ingram, H.C. Kaestli, D. Kotlinski, C. Lange, M. Missiroli[63], L. Noehte[63], T. Rohe, A. Samalan

PSI Center for Neutron and Muon Sciences, Villigen, Switzerland

T.K. Aarrestad, K. Androsov[61], M. Backhaus, G. Bonomelli, A. Calandri, C. Cazzaniga, K. Datta, P. De Bryas Dexmiers D'archiac[61], A. De Cosa, G. Dissertori, M. Dittmar, M. Donegà, F. Eble, M. Galli, K. Gedia, F. Glessgen, C. Grab, N. Härringer, T.G. Harte, D. Hits, W. Lustermann, A.-M. Lyon, R.A. Manzoni, M. Marchegiani, L. Marchese, C. Martin Perez, A. Mascellani[61], F. Nessi-Tedaldi, F. Pauss, V. Perovic, S. Pigazzini, B. Ristic, F. Riti, R. Seidita, J. Steggemann[61], A. Tarabini, D. Valsecchi, R. Wallny

ETH Zurich - Institute for Particle Physics and Astrophysics (IPA), Zurich, Switzerland

C. Amsler[64], P. Bärtschi, M.F. Canelli, K. Cormier, M. Huwiler, W. Jin, A. Jofrehei, B. Kilminster, S. Leontsinis, S.P. Liechti, A. Macchiolo, P. Meiring, F. Meng, U. Molinatti, J. Motta, A. Reimers, P. Robmann, M. Senger, E. Shokr, F. Stäger, R. Tramontano

Universität Zürich, Zurich, Switzerland

C. Adloff[65], D. Bhowmik, C.M. Kuo, W. Lin, P.K. Rout, P.C. Tiwari[39], S.S. Yu

National Central University, Chung-Li, Taiwan

L. Ceard, K.F. Chen, P.s. Chen, Z.g. Chen, A. De Iorio, W.-S. Hou, T.h. Hsu, Y.w. Kao, S. Karmakar, G. Kole, Y.y. Li, R.-S. Lu, E. Paganis, X.f. Su, J. Thomas-Wilsker, L.s. Tsai, D. Tsionou, H.y. Wu, E. Yazgan

National Taiwan University (NTU), Taipei, Taiwan

C. Asawatangtrakuldee, N. Srimanobhas, V. Wachirapusitanand

High Energy Physics Research Unit, Department of Physics, Faculty of Science, Chulalongkorn University, Bangkok, Thailand

D. Agyel, F. Boran, F. Dolek, I. Dumanoglu[66], E. Eskut, Y. Guler[67], E. Gurpinar Guler[67], C. Isik, O. Kara, A. Kayis Topaksu, U. Kiminsu, G. Onengut, K. Ozdemir[68], A. Polatoz, B. Tali[69], U.G. Tok, S. Turkcapar, E. Uslan, I.S. Zorbakir

Çukurova University, Physics Department, Science and Art Faculty, Adana, Turkey

G. Sokmen, M. Yalvac[70]

Middle East Technical University, Physics Department, Ankara, Turkey

B. Akgun, I.O. Atakisi, E. Gülmez, M. Kaya[71], O. Kaya[72], S. Tekten[73]

Bogazici University, Istanbul, Turkey

A. Cakir, K. Cankocak[66,74], G.G. Dincer[66], Y. Komurcu, S. Sen[75]

Istanbul Technical University, Istanbul, Turkey

O. Aydilek[76], B. Hacisahinoglu, I. Hos[77], B. Kaynak, S. Ozkorucuklu, O. Potok, H. Sert, C. Simsek, C. Zorbilmez

Istanbul University, Istanbul, Turkey

S. Cerci, B. Isildak[78], D. Sunar Cerci, T. Yetkin

Yildiz Technical University, Istanbul, Turkey

A. Boyaryntsev, B. Grynyov

Institute for Scintillation Materials of National Academy of Science of Ukraine, Kharkiv, Ukraine

L. Levchuk

National Science Centre, Kharkiv Institute of Physics and Technology, Kharkiv, Ukraine

D. Anthony, J.J. Brooke, A. Bundock, F. Bury, E. Clement, D. Cussans, H. Flacher, M. Glowacki, J. Goldstein, H.F. Heath, M.-L. Holmberg, L. Kreczko, S. Paramesvaran, L. Robertshaw, S. Seif El Nasr-Storey, V.J. Smith, N. Stylianou[79], K. Walkingshaw Pass

University of Bristol, Bristol, United Kingdom

A.H. Ball, K.W. Bell, A. Belyaev[80], C. Brew, R.M. Brown, D.J.A. Cockerill, C. Cooke, A. Elliot, K.V. Ellis, K. Harder, S. Harper, J. Linacre, K. Manolopoulos, D.M. Newbold, E. Olaiya, D. Petyt, T. Reis, A.R. Sahasransu, G. Salvi, T. Schuh, C.H. Shepherd-Themistocleous, I.R. Tomalin, K.C. Whalen, T. Williams

Rutherford Appleton Laboratory, Didcot, United Kingdom

I. Andreou, R. Bainbridge, P. Bloch, C.E. Brown, O. Buchmuller, V. Cacchio, C.A. Carrillo Montoya, G.S. Chahal[81], D. Colling, J.S. Dancu, I. Das, P. Dauncey, G. Davies, J. Davies, M. Della Negra, S. Fayer, G. Fedi, G. Hall, M.H. Hassanshahi, A. Howard, G. Iles, C.R. Knight, J. Langford, J. León Holgado, L. Lyons, A.-M. Magnan, B. Maier, S. Mallios, M. Mieskolainen, J. Nash[82], M. Pesaresi, P.B. Pradeep, B.C. Radburn-Smith, A. Richards, A. Rose, K. Savva, C. Seez,

R. Shukla, A. Tapper, K. Uchida, G.P. Uttley, L.H. Vage, T. Virdee[31], M. Vojinovic, N. Wardle, D. Winterbottom

Imperial College, London, United Kingdom

J.E. Cole, A. Khan, P. Kyberd, I.D. Reid

Brunel University, Uxbridge, United Kingdom

S. Abdullin, A. Brinkerhoff, E. Collins, M.R. Darwish[83], J. Dittmann, K. Hatakeyama, J. Hiltbrand, B. McMaster, J. Samudio, S. Sawant, C. Sutantawibul, J. Wilson

Baylor University, Waco, TX, USA

R. Bartek, A. Dominguez, C. Huerta Escamilla, A.E. Simsek, R. Uniyal, A.M. Vargas Hernandez

Catholic University of America, Washington, DC, USA

B. Bam, A. Buchot Perraguin, R. Chudasama, S.I. Cooper, C. Crovella, S.V. Gleyzer, E. Pearson, C.U. Perez, P. Rumerio[84], E. Usai, R. Yi

The University of Alabama, Tuscaloosa, AL, USA

A. Akpinar, C. Cosby, G. De Castro, Z. Demiragli, C. Erice, C. Fangmeier, C. Fernandez Madrazo, E. Fontanesi, D. Gastler, F. Golf, S. Jeon, J. O'cain, I. Reed, J. Rohlf, K. Salyer, D. Sperka, D. Spitzbart, I. Suarez, A. Tsatsos, A.G. Zecchinelli

Boston University, Boston, MA, USA

G. Benelli, D. Cutts, L. Gouskos, M. Hadley, U. Heintz, J.M. Hogan[85], T. Kwon, G. Landsberg, K.T. Lau, D. Li, J. Luo, S. Mondal, N. Pervan, T. Russell, S. Sagir[86], X. Shen, F. Simpson, M. Stamenkovic, N. Venkatasubramanian, X. Yan

Brown University, Providence, RI, USA

S. Abbott, C. Brainerd, R. Breedon, H. Cai, M. Calderon De La Barca Sanchez, M. Chertok, M. Citron, J. Conway, P.T. Cox, R. Erbacher, F. Jensen, O. Kukral, G. Mocellin, M. Mulhearn, S. Ostrom, W. Wei, S. Yoo, F. Zhang

University of California, Davis, Davis, CA, USA

M. Bachtis, R. Cousins, A. Datta, G. Flores Avila, J. Hauser, M. Ignatenko, M.A. Iqbal, T. Lam, E. Manca, A. Nunez Del Prado, D. Saltzberg, V. Valuev

University of California, Los Angeles, CA, USA

R. Clare, J.W. Gary, M. Gordon, G. Hanson, W. Si

University of California, Riverside, Riverside, CA, USA

A. Aportela, A. Arora, J.G. Branson, S. Cittolin, S. Cooperstein, D. Diaz, J. Duarte, L. Giannini, Y. Gu, J. Guiang, R. Kansal, V. Krutelyov, R. Lee, J. Letts, M. Masciovecchio, F. Mokhtar, S. Mukherjee, M. Pieri, M. Quinnan, B.V. Sathia Narayanan, V. Sharma, M. Tadel, E. Vourliotis, F. Würthwein, Y. Xiang, A. Yagil

University of California, San Diego, La Jolla, CA, USA

A. Barzdukas, L. Brennan, C. Campagnari, K. Downham, C. Grieco, J. Incandela, J. Kim, A.J. Li, P. Masterson, H. Mei, J. Richman, S.N. Santpur, U. Sarica, R. Schmitz, F. Setti, J. Sheplock, D. Stuart, T.Á. Vámi, S. Wang, D. Zhang

University of California, Santa Barbara - Department of Physics, Santa Barbara, CA, USA

S. Bhattacharya, A. Bornheim, O. Cerri, A. Latorre, J. Mao, H.B. Newman, G. Reales Gutiérrez, M. Spiropulu, J.R. Vlimant, C. Wang, S. Xie, R.Y. Zhu

California Institute of Technology, Pasadena, CA, USA

J. Alison, S. An, P. Bryant, M. Cremonesi, V. Dutta, T. Ferguson, T.A. Gómez Espinosa, A. Harilal, A. Kallil Tharayil, C. Liu, T. Mudholkar, S. Murthy, P. Palit, K. Park, M. Paulini, A. Roberts, A. Sanchez, W. Terrill

Carnegie Mellon University, Pittsburgh, PA, USA

J.P. Cumalat, W.T. Ford, A. Hart, A. Hassani, G. Karathanasis, N. Manganelli, J. Pearkes, C. Savard, N. Schonbeck, K. Stenson, K.A. Ulmer, S.R. Wagner, N. Zipper, D. Zuolo

University of Colorado Boulder, Boulder, CO, USA

J. Alexander, S. Bright-Thonney, X. Chen, D.J. Cranshaw, J. Fan, X. Fan, S. Hogan, P. Kotamnives, J. Monroy, M. Oshiro, J.R. Patterson, M. Reid, A. Ryd, J. Thom, P. Wittich, R. Zou

Cornell University, Ithaca, NY, USA

M. Albrow, M. Alyari, O. Amram, G. Apollinari, A. Apresyan, L.A.T. Bauerdick, D. Berry, J. Berryhill, P.C. Bhat, K. Burkett, J.N. Butler, A. Canepa, G.B. Cerati, H.W.K. Cheung, F. Chlebana, G. Cummings, J. Dickinson, I. Dutta, V.D. Elvira, Y. Feng, J. Freeman, A. Gandrakota, Z. Gecse, L. Gray, D. Green, A. Grummer, S. Grünendahl, D. Guerrero, O. Gutsche, R.M. Harris, R. Heller, T.C. Herwig, J. Hirschauer, B. Jayatilaka, S. Jindariani, M. Johnson, U. Joshi, T. Klijnsma, B. Klima, K.H.M. Kwok, S. Lammel, D. Lincoln, R. Lipton, T. Liu, C. Madrid, K. Maeshima, C. Mantilla, D. Mason, P. McBride, P. Merkel, S. Mrenna, S. Nahn, J. Ngadiuba, D. Noonan, S. Norberg, V. Papadimitriou, N. Pastika, K. Pedro, C. Pena[87], F. Ravera, A. Reinsvold Hall[88], L. Ristori, M. Safdari, E. Sexton-Kennedy, N. Smith, A. Soha, L. Spiegel, S. Stoynev, J. Strait, L. Taylor, S. Tkaczyk, N.V. Tran, L. Uplegger, E.W. Vaandering, I. Zoi

Fermi National Accelerator Laboratory, Batavia, IL, USA

C. Aruta, P. Avery, D. Bourilkov, P. Chang, V. Cherepanov, R.D. Field, C. Huh, E. Koenig, M. Kolosova, J. Konigsberg, A. Korytov, K. Matchev, N. Menendez, G. Mitselmakher, K. Mohrman, A. Muthirakalayil Madhu, N. Rawal, S. Rosenzweig, Y. Takahashi, J. Wang

University of Florida, Gainesville, FL, USA

T. Adams, A. Al Kadhim, A. Askew, S. Bower, V. Hagopian, R. Hashmi, R.S. Kim, S. Kim, T. Kolberg, G. Martinez, H. Prosper, P.R. Prova, M. Wulansatiti, R. Yohay, J. Zhang

Florida State University, Tallahassee, FL, USA

B. Alsufyani, M.M. Baarmand, S. Butalla, S. Das, T. Elkafrawy[19], M. Hohlmann, E. Yanes

Florida Institute of Technology, Melbourne, FL, USA

M.R. Adams, A. Baty, C. Bennett, R. Cavanaugh, R. Escobar Franco, O. Evdokimov, C.E. Gerber, M. Hawksworth, A. Hingrajiya, D.J. Hofman, J.h. Lee, D.S. Lemos, A.H. Merrit, C. Mills, S. Nanda, G. Oh, B. Ozek, D. Pilipovic, R. Pradhan, E. Prifti, T. Roy, S. Rudrabhatla, N. Singh, M.B. Tonjes, N. Varelas, M.A. Wadud, Z. Ye, J. Yoo

University of Illinois Chicago, Chicago, IL, USA

M. Alhusseini, D. Blend, K. Dilsiz [89], L. Emediato, G. Karaman, O.K. Köseyan, J.-P. Merlo, A. Mestvirishvili [90], O. Neogi, H. Ogul [91], Y. Onel, A. Penzo, C. Snyder, E. Tiras [92]

The University of Iowa, Iowa City, IA, USA

B. Blumenfeld, L. Corcodilos, J. Davis, A.V. Gritsan, L. Kang, S. Kyriacou, P. Maksimovic, M. Roguljic, J. Roskes, S. Sekhar, M. Swartz

Johns Hopkins University, Baltimore, MD, USA

A. Abreu, L.F. Alcerro Alcerro, J. Anguiano, S. Arteaga Escatel, P. Baringer, A. Bean, Z. Flowers, D. Grove, J. King, G. Krintiras, M. Lazarovits, C. Le Mahieu, J. Marquez, M. Murray, M. Nickel, M. Pitt, S. Popescu [93], C. Rogan, C. Royon, R. Salvatico, S. Sanders, C. Smith, G. Wilson

The University of Kansas, Lawrence, KS, USA

B. Allmond, R. Gujju Gurunadha, A. Ivanov, K. Kaadze, Y. Maravin, J. Natoli, D. Roy, G. Sorrentino

Kansas State University, Manhattan, KS, USA

A. Baden, A. Belloni, J. Bistany-riebman, Y.M. Chen, S.C. Eno, N.J. Hadley, S. Jabeen, R.G. Kellogg, T. Koeth, B. Kronheim, Y. Lai, S. Lascio, A.C. Mignerey, S. Nabili, C. Palmer, C. Papageorgakis, M.M. Paranjpe, E. Popova [94], A. Shevelev, L. Wang

University of Maryland, College Park, MD, USA

J. Bendavid, I.A. Cali, P.c. Chou, M. D'Alfonso, J. Eysermans, C. Freer, G. Gomez-Ceballos, M. Goncharov, G. Grosso, P. Harris, D. Hoang, D. Kovalskyi, J. Krupa, L. Lavezzo, Y.-J. Lee, K. Long, C. Mcginn, A. Novak, C. Paus, C. Reissel, C. Roland, G. Roland, S. Rothman, G.S.F. Stephans, Z. Wang, B. Wyslouch, T.J. Yang

Massachusetts Institute of Technology, Cambridge, MA, USA

B. Crossman, B.M. Joshi, C. Kapsiak, M. Krohn, D. Mahon, J. Mans, B. Marzocchi, M. Revering, R. Rusack, R. Saradhy, N. Strobbe

University of Minnesota, Minneapolis, MN, USA

K. Bloom, D.R. Claes, G. Haza, J. Hossain, C. Joo, I. Kravchenko, J.E. Siado, W. Tabb, A. Vagnerini, A. Wightman, F. Yan, D. Yu

University of Nebraska-Lincoln, Lincoln, NE, USA

H. Bandyopadhyay, L. Hay, H.w. Hsia, I. Iashvili, A. Kalogeropoulos, A. Kharchilava, M. Morris, D. Nguyen, J. Pekkanen, S. Rappoccio, H. Rejeb Sfar, A. Williams, P. Young

State University of New York at Buffalo, Buffalo, NY, USA

G. Alverson, E. Barberis, J. Bonilla, M. Campana, J. Dervan, Y. Haddad, Y. Han, A. Krishna, J. Li, M. Lu, G. Madigan, R. Mccarthy, D.M. Morse, V. Nguyen, T. Orimoto, A. Parker, L. Skinnari, D. Wood

Northeastern University, Boston, MA, USA

J. Bueghly, S. Dittmer, K.A. Hahn, Y. Liu, Y. Miao, D.G. Monk, M.H. Schmitt, A. Taliercio, M. Velasco

Northwestern University, Evanston, IL, USA

G. Agarwal, R. Band, R. Bucci, S. Castells, A. Das, R. Goldouzian, M. Hildreth, K.W. Ho, K. Hurtado Anampa, T. Ivanov, C. Jessop, K. Lannon, J. Lawrence, N. Loukas, L. Lutton, J. Mariano, N. Marinelli, I. Mcalister, T. McCauley, C. Mcgrady, C. Moore, Y. Musienko[24], H. Nelson, M. Osherson, A. Piccinelli, R. Ruchti, A. Townsend, Y. Wan, M. Wayne, H. Yockey, M. Zarucki, L. Zygala

University of Notre Dame, Notre Dame, IN, USA

A. Basnet, B. Bylsma, M. Carrigan, L.S. Durkin, C. Hill, M. Joyce, M. Nunez Ornelas, K. Wei, B.L. Winer, B.R. Yates

The Ohio State University, Columbus, OH, USA

H. Bouchamaoui, K. Coldham, P. Das, G. Dezoort, P. Elmer, A. Frankenthal, B. Greenberg, N. Haubrich, K. Kennedy, G. Kopp, S. Kwan, D. Lange, A. Loeliger, D. Marlow, I. Ojalvo, J. Olsen, D. Stickland, C. Tully

Princeton University, Princeton, NJ, USA

S. Malik

University of Puerto Rico, Mayaguez, PR, USA

A.S. Bakshi, S. Chandra, R. Chawla, A. Gu, L. Gutay, M. Jones, A.W. Jung, A.M. Koshy, M. Liu, G. Negro, N. Neumeister, G. Paspalaki, S. Piperov, V. Scheurer, J.F. Schulte, M. Stojanovic, J. Thieman, A.K. Virdi, F. Wang, A. Wildridge, W. Xie, Y. Yao

Purdue University, West Lafayette, IN, USA

J. Dolen, N. Parashar, A. Pathak

Purdue University Northwest, Hammond, IN, USA

D. Acosta, T. Carnahan, K.M. Ecklund, P.J. Fernández Manteca, S. Freed, P. Gardner, F.J.M. Geurts, I. Krommydas, W. Li, J. Lin, O. Miguel Colin, B.P. Padley, R. Redjimi, J. Rotter, E. Yigitbasi, Y. Zhang

Rice University, Houston, TX, USA

A. Bodek, P. de Barbaro, R. Demina, J.L. Dulemba, A. Garcia-Bellido, O. Hindrichs, A. Khukhunaishvili, N. Parmar, P. Parygin[94], R. Taus

University of Rochester, Rochester, NY, USA

B. Chiarito, J.P. Chou, S.V. Clark, D. Gadkari, Y. Gershtein, E. Halkiadakis, M. Heindl, C. Houghton, D. Jaroslawski, S. Konstantinou, I. Laflotte, A. Lath, R. Montalvo, K. Nash, J. Reichert, H. Routray, P. Saha, S. Salur, S. Schnetzer, S. Somalwar, R. Stone, S.A. Thayil, S. Thomas, J. Vora, H. Wang

Rutgers, The State University of New Jersey, Piscataway, NJ, USA

D. Ally, A.G. Delannoy, S. Fiorendi, S. Higginbotham, T. Holmes, A.R. Kanuganti, N. Karunarathna, L. Lee, E. Nibigira, S. Spanier

University of Tennessee, Knoxville, TN, USA

D. Aebi, M. Ahmad, T. Akhter, O. Bouhali[95], R. Eusebi, J. Gilmore, T. Huang, T. Kamon[96], H. Kim, S. Luo, R. Mueller, D. Overton, D. Rathjens, A. Safonov

Texas A&M University, College Station, TX, USA

N. Akchurin, J. Damgov, N. Gogate, V. Hegde, A. Hussain, Y. Kazhykarim, K. Lamichhane, S.W. Lee, A. Mankel, T. Peltola, I. Volobouev

Texas Tech University, Lubbock, TX, USA

E. Appelt, Y. Chen, S. Greene, A. Gurrola, W. Johns, R. Kunnawalkam Elayavalli, A. Melo, F. Romeo, P. Sheldon, S. Tuo, J. Velkovska, J. Viinikainen

Vanderbilt University, Nashville, TN, USA

B. Cardwell, H. Chung, B. Cox, J. Hakala, R. Hirosky, A. Ledovskoy, C. Neu

University of Virginia, Charlottesville, VA, USA

S. Bhattacharya, P.E. Karchin

Wayne State University, Detroit, MI, USA

A. Aravind, S. Banerjee, K. Black, T. Bose, S. Dasu, I. De Bruyn, P. Everaerts, C. Galloni, H. He, M. Herndon, A. Herve, C.K. Koraka, A. Lanaro, R. Loveless, J. Madhusudanan Sreekala, A. Mallampalli, A. Mohammadi, S. Mondal, G. Parida, L. Pétré, D. Pinna, A. Savin, V. Shang, V. Sharma, W.H. Smith, D. Teague, H.F. Tsoi, W. Vetens, A. Warden

University of Wisconsin - Madison, Madison, WI, USA

S. Afanasiev, V. Alexakhin, D. Budkouski, I. Golutvin[†], I. Gorbunov, V. Karjavine, V. Korenkov, A. Lanev, A. Malakhov, V. Matveev[97], V. Palichik, V. Perelygin, M. Savina, V. Shalaev, S. Shmatov, S. Shulha, V. Smirnov, O. Teryaev, N. Voytishin, B.S. Yuldashev[98], A. Zarubin, I. Zhizhin, Yu. Andreev, A. Dermenev, S. Gninenko, N. Golubev, A. Karneyeu, D. Kirpichnikov, M. Kirsanov, N. Krasnikov, I. Tlisova, A. Toropin

Authors affiliated with an international laboratory covered by a cooperation agreement with CERN

G. Gavrilov, V. Golovtcov, Y. Ivanov, V. Kim[99], P. Levchenko[100], V. Murzin, V. Oreshkin, D. Sosnov, V. Sulimov, L. Uvarov, A. Vorobyev[†], T. Aushev, V. Gavrilov, N. Lychkovskaya, A. Nikitenko[101,102], V. Popov, A. Zhokin, M. Chadeeva[99], R. Chistov[99], S. Polikarpov[99], V. Andreev, M. Azarkin, M. Kirakosyan, A. Terkulov, E. Boos, V. Bunichev, M. Dubinin[87], L. Dudko, V. Klyukhin, O. Kodolova[102], O. Lukina, S. Obraztsov, M. Perfilov, V. Savrin, A. Snigirev, G. Vorotnikov, V. Blinov[99], T. Dimova[99], A. Kozyrev[99], O. Radchenko[99], Y. Skovpen[99], V. Kachanov, D. Konstantinov, S. Slabospitskii, A. Uzunian, A. Babaev, V. Borshch, D. Druzhkin[103], V. Makarenko, T. Nechaeva

Authors affiliated with an institute formerly covered by a cooperation agreement with CERN

[†] Deceased.
[1] Also at Yerevan State University, Yerevan, Armenia.
[2] Also at TU Wien, Vienna, Austria.
[3] Also at Ghent University, Ghent, Belgium.
[4] Also at Universidade do Estado do Rio de Janeiro, Rio de Janeiro, Brazil.
[5] Also at Universidade Estadual de Campinas, Campinas, Brazil.
[6] Also at Federal University of Rio Grande do Sul, Porto Alegre, Brazil.
[7] Also at UFMS, Nova Andradina, Brazil.
[8] Also at Nanjing Normal University, Nanjing, China.
[9] Now at The University of Iowa, Iowa City, Iowa, USA.
[10] Also at University of Chinese Academy of Sciences, Beijing, China.
[11] Also at China Center of Advanced Science and Technology, Beijing, China.
[12] Also at University of Chinese Academy of Sciences, Beijing, China.
[13] Also at China Spallation Neutron Source, Guangdong, China.
[14] Now at Henan Normal University, Xinxiang, China.
[15] Also at Université Libre de Bruxelles, Bruxelles, Belgium.
[16] Also at an institute formerly covered by a cooperation agreement with CERN.
[17] Now at British University in Egypt, Cairo, Egypt.
[18] Also at Zewail City of Science and Technology, Zewail, Egypt.

[19] Now at Ain Shams University, Cairo, Egypt.
[20] Also at Purdue University, West Lafayette, Indiana, USA.
[21] Also at Université de Haute Alsace, Mulhouse, France.
[22] Also at Istinye University, Istanbul, Turkey.
[23] Also at Tbilisi State University, Tbilisi, Georgia.
[24] Also at an international laboratory covered by a cooperation agreement with CERN.
[25] Also at The University of the State of Amazonas, Manaus, Brazil.
[26] Also at University of Hamburg, Hamburg, Germany.
[27] Also at RWTH Aachen University, III. Physikalisches Institut A, Aachen, Germany.
[28] Also at Bergische University Wuppertal (BUW), Wuppertal, Germany.
[29] Also at Brandenburg University of Technology, Cottbus, Germany.
[30] Also at Forschungszentrum Jülich, Juelich, Germany.
[31] Also at CERN, European Organization for Nuclear Research, Geneva, Switzerland.
[32] Also at HUN-REN ATOMKI - Institute of Nuclear Research, Debrecen, Hungary.
[33] Now at Universitatea Babes-Bolyai - Facultatea de Fizica, Cluj-Napoca, Romania.
[34] Also at MTA-ELTE Lendület CMS Particle and Nuclear Physics Group, Eötvös Loránd University, Budapest, Hungary.
[35] Also at HUN-REN Wigner Research Centre for Physics, Budapest, Hungary.
[36] Also at Physics Department, Faculty of Science, Assiut University, Assiut, Egypt.
[37] Also at Punjab Agricultural University, Ludhiana, India.
[38] Also at University of Visva-Bharati, Santiniketan, India.
[39] Also at Indian Institute of Science (IISc), Bangalore, India.
[40] Also at IIT Bhubaneswar, Bhubaneswar, India.
[41] Also at Institute of Physics, Bhubaneswar, India.
[42] Also at University of Hyderabad, Hyderabad, India.
[43] Also at Deutsches Elektronen-Synchrotron, Hamburg, Germany.
[44] Also at Isfahan University of Technology, Isfahan, Iran.
[45] Also at Sharif University of Technology, Tehran, Iran.
[46] Also at Department of Physics, University of Science and Technology of Mazandaran, Behshahr, Iran.
[47] Also at Department of Physics, Isfahan University of Technology, Isfahan, Iran.
[48] Also at Department of Physics, Faculty of Science, Arak University, ARAK, Iran.
[49] Also at Helwan University, Cairo, Egypt.
[50] Also at Italian National Agency for New Technologies, Energy and Sustainable Economic Development, Bologna, Italy.
[51] Also at Centro Siciliano di Fisica Nucleare e di Struttura Della Materia, Catania, Italy.
[52] Also at Università degli Studi Guglielmo Marconi, Roma, Italy.
[53] Also at Scuola Superiore Meridionale, Università di Napoli 'Federico II', Napoli, Italy.
[54] Also at Fermi National Accelerator Laboratory, Batavia, Illinois, USA.
[55] Also at Consiglio Nazionale delle Ricerche - Istituto Officina dei Materiali, Perugia, Italy.
[56] Also at Department of Applied Physics, Faculty of Science and Technology, Universiti Kebangsaan Malaysia, Bangi, Malaysia.
[57] Also at Consejo Nacional de Ciencia y Tecnología, Mexico City, Mexico.
[58] Also at Trincomalee Campus, Eastern University, Sri Lanka, Nilaveli, Sri Lanka.
[59] Also at Saegis Campus, Nugegoda, Sri Lanka.
[60] Also at National and Kapodistrian University of Athens, Athens, Greece.
[61] Also at Ecole Polytechnique Fédérale Lausanne, Lausanne, Switzerland.
[62] Also at University of Vienna, Vienna, Austria.
[63] Also at Universität Zürich, Zurich, Switzerland.
[64] Also at Stefan Meyer Institute for Subatomic Physics, Vienna, Austria.
[65] Also at Laboratoire d'Annecy-le-Vieux de Physique des Particules, IN2P3-CNRS, Annecy-le-Vieux, France.
[66] Also at Near East University, Research Center of Experimental Health Science, Mersin, Turkey.
[67] Also at Konya Technical University, Konya, Turkey.
[68] Also at Izmir Bakircay University, Izmir, Turkey.
[69] Also at Adiyaman University, Adiyaman, Turkey.
[70] Also at Bozok Universitetesi Rektörlügü, Yozgat, Turkey.
[71] Also at Marmara University, Istanbul, Turkey.
[72] Also at Milli Savunma University, Istanbul, Turkey.
[73] Also at Kafkas University, Kars, Turkey.
[74] Now at Istanbul Okan University, Istanbul, Turkey.
[75] Also at Hacettepe University, Ankara, Turkey.
[76] Also at Erzincan Binali Yildirim University, Erzincan, Turkey.
[77] Also at Istanbul University - Cerrahpasa, Faculty of Engineering, Istanbul, Turkey.
[78] Also at Yildiz Technical University, Istanbul, Turkey.
[79] Also at Vrije Universiteit Brussel, Brussel, Belgium.
[80] Also at School of Physics and Astronomy, University of Southampton, Southampton, United Kingdom.
[81] Also at IPPP Durham University, Durham, United Kingdom.
[82] Also at Monash University, Faculty of Science, Clayton, Australia.
[83] Also at Institute of Basic and Applied Sciences, Faculty of Engineering, Arab Academy for Science, Technology and Maritime Transport, Alexandria, Egypt.
[84] Also at Università di Torino, Torino, Italy.
[85] Also at Bethel University, St. Paul, Minnesota, USA.
[86] Also at Karamanoğlu Mehmetbey University, Karaman, Turkey.
[87] Also at California Institute of Technology, Pasadena, California, USA.
[88] Also at United States Naval Academy, Annapolis, Maryland, USA.
[89] Also at Bingol University, Bingol, Turkey.
[90] Also at Georgian Technical University, Tbilisi, Georgia.
[91] Also at Sinop University, Sinop, Turkey.
[92] Also at Erciyes University, Kayseri, Turkey.
[93] Also at Horia Hulubei National Institute of Physics and Nuclear Engineering (IFIN-HH), Bucharest, Romania.
[94] Now at another institute formerly covered by a cooperation agreement with CERN.
[95] Also at Texas A&M University at Qatar, Doha, Qatar.
[96] Also at Kyungpook National University, Daegu, Korea.
[97] Also at another international laboratory covered by a cooperation agreement with CERN.
[98] Also at Institute of Nuclear Physics of the Uzbekistan Academy of Sciences, Tashkent, Uzbekistan.

[99] Also at another institute formerly covered by a cooperation agreement with CERN.
[100] Also at Northeastern University, Boston, Massachusetts, USA.
[101] Also at Imperial College, London, United Kingdom.
[102] Now at Yerevan Physics Institute, Yerevan, Armenia.
[103] Also at Universiteit Antwerpen, Antwerpen, Belgium.